2017

An investigation on the thermophysical properties of a binary molten salt system containing both aluminum oxide and titanium oxide nanoparticle suspensions

Kunal Giridhar

ABSTRACT

AN INVESTIGATION ON THE THERMOPHYSICAL PROPERTIES OF A BINARY MOLTEN SALT SYSTEM CONTAINING BOTH ALUMINUM OXIDE AND TITANIUM OXIDE NANOPARTICLE SUSPENSIONS

Kunal Giridhar, MS
Department of Mechanical Engineering
Northern Illinois University, 2017
Dr. John Shelton, Director

Molten salts are showing great potential to replace current heat transfer and thermal energy storage fluids in concentrated solar plants because of their capability to maximize thermal energy storage, greater stability, cost effectiveness and significant thermal properties. However one of the major drawbacks of using molten salt as heat transfer fluid is that they are in solid state at room temperature and they have a high freezing point. Hence, significant resources would be required to maintain it in liquid form. If molten salt freezes while in operation, it would eventually damage piping network due to its volume shrinkage along with rendering the entire plant inoperable. It is long known that addition of nanoparticle suspensions has led to significant changes in thermal properties of fluids. In this investigation, aluminum oxide and titanium oxide nanoparticles of varying concentrations are added to molten salt/solar salt system consisting of 60% sodium nitrate and 40% potassium nitrate. Using differential scanning calorimeter, an attempt will be made to investigate changes in heat capacity of system, depression in freezing point and changes in latent heat of fusion. Scanning electron microscope will be used to take images of samples to study changes in microstructure of mixture, ensure uniform distribution of nanoparticle in system and verify authenticity of materials used for experimentation.

Due to enormous magnitude of CSP plant, actual implementation of molten salt system is on a large scale. With this investigation, even microscopic enhancement in heat capacity and slight lowering of freezing point will lead to greater benefits in terms of efficiency and cost of operation of plant. These results will further the argument for viability of molten salt as a heat transfer fluid and thermal storage system in CSP. One of the objective of this experimentation is to also collect experimental data which can be used for establishing relation between concentration of nanoparticles and change in thermophysical properties of molten salt for various types of nanoparticles.

NORTHERN ILLINOIS UNIVERSITY
DEKALB, ILLINOIS

MAY 2017

AN INVESTIGATION ON THE THERMOPHYSICAL PROPERTIES OF A BINARY MOLTEN SALT SYSTEM CONTAINING BOTH ALUMINUM OXIDE AND TITANIUM OXIDE NANOPARTICLE SUSPENSIONS

BY

KUNAL GIRIDHAR

A THESIS SUBMITTED TO THE GRADUATE SCHOOL

IN PARTIAL FULFILLMENT OF THE REQUIREMENTS

FOR THE DEGREE

MASTER OF SCIENCE

DEPARTMENT OF MECHANICAL ENGINEERING

Thesis Director:
Dr. John Shelton

ACKNOWLEDGEMENTS

I would first like to thank Dr. John Shelton for all his guidance and efforts to steer me in right direction. His hard work and perseverance has provided a guided path for the project to move forward in times of concern and make this work a success. I would also like to thank committee members, Dr. Pradip Majumdar and Dr. Sahar Vahabzadeh for their valuable inputs to this work which always provided a diverse approach and made this work more effective.

I would like to thank Mechanical Engineering Department, College of Engineering and Northern Illinois University for providing access to all their resources required for successful completion of this thesis. I would also like to thank Argonne National Laboratory for providing admittance to its world class research facility and allowing access to SEM equipment in their premises for our research work. I would like to thank my colleagues for guiding and helping me with this work and also for accommodating my requests.

Finally, I would like to express my sincere gratitude towards my parents, family and friends for providing continuous encouragement, assistance and support throughout my journey as a student and researcher. My work would have not been possible without them. Thank you.

Kunal Manoj Giridhar.

TABLE OF CONTENTS

Page

LIST OF TABLES

Page

LIST OF FIGURES

Chapter 1

INTRODUCTION

1.1 Solar Energy

Renewable energy currently has a share of 2.77% of total consumption of energy. The significance of replacing the use of fossil fuel by renewable energy has been long accepted. Many surveys predict that renewable energy and natural gas are going to be major contributors in race to meet energy requirements of world until 2040 [1] The detail analysis shows that in next 25 years the fossil fuels contribution in energy sector will reduce to a low level and renewable energy share will almost double its present share [1].

According to Dr. Fatih Birol, the IEA‘s Executive Director, natural gas will be the clear winner for next 25 years but wind and solar will replace coal, the champion of previous 25 years. Also it is necessary to increase use of renewable energy to achieve our climate goals. As the reserves of fossil fuels are finishing fast and because the harmful gas emissions have adverse effects on global environment, the need for renewable and clean energy has increased. Considering above analysis, solar energy stands out to be most promising substitute to fossil fuels.

The energy from sunlight, wind, rain, tides, waves and geothermal heat is termed as renewable energy. Solar energy is most important renewable energy source and International Energy Agency has projected that solar power could provide a third of the global final energy demand after 2060 and CO_2 emissions would be then reduced to very low levels.

Solar energy is abundantly available free of cost in majority regions of the world. The United Nations Development Program in its 2000 World Energy Assessment found that the annual potential of solar energy was 1575 exajoules (minimum) to 49837 exajoules (EJ) (maximum), which is many times more than the world energy consumption today. Sun is a very large perennial source of energy. The sunlight incident on earth's surface intercepts about 1.8 x 10^{11} MW of power. Most of the world's population lives in areas where 150 – 300 watts/m^2 solar energy is available. Solar thermal energy technologies can be used for water heating, space heating, space cooling and process heat generation.

1.2 Concentrated Solar Power Plants (CSP).

Solar power is use of solar energy for production of electricity. Electricity is produced from sunlight by using concentrated solar power (CSP) or by photovoltaics (PV). It has been projected that, by 2050, energy from CSP and PV would contribute about 11 and 16 percent, respectively, of the total electricity consumption worldwide [1]. It has also projected that solar would be the world's largest source of electricity at that time. World's first solar thermal power station was built in Maadi, Egypt between 1912 and 1913 [2].

Today CSP plants are used for electricity generation. CSP systems use lenses or mirrors and tracking systems to focus a large area of sunlight into a small beam, this concentrates the solar energy in small area. Different concentrating technologies like parabolic trough, compact linear Fresnel reflector, sterling dish and solar power tower are being developed. This concentrated heat is used to heat a working fluid known as heat transfer fluid (HTF). As solar energy is not available continuously the heat is stored in thermal energy storage (TES) systems.

Because of thermal storage the electricity can be generated during night and cloudy days also. This energy is then used for steam generation, which in turn drives steam turbines. Steam turbines are coupled to generators which produce electrical power.

First commercial CSP was developed in 1980. The world's largest CSP plant is Ivanpah Solar power facility (392 MW) in California's Mojave Dessert. The three other main CSP plants are Solnava Solar Power Station (150 MW), Andasol Solar Power Station (150 MW) and Extresol Solar Power Station (150MW) located in Spain [2].

Today CSP produces approximately 3.5 GW all around the world annually. The important point is that this technology can be retrofitted in the existing power plants which use coal or oil fuels because the process of generating electricity is same, which is by using steam turbines, coupled to the generators. The cost of electricity in CSP is roughly twice as much as electricity from a coal fired power plant. The cost of building a CSP station is higher but the fuel is free. All the efforts are being made to increase the efficiency of CSP plant. Improvement in Thermal Energy Storage systems plays most important role in increasing the efficiency and reducing the cost of CSP plant [3].

1.3 Overview of Heat Transfer Fluids and Thermal Energy Storage Fluids in CSP.

1.3.1 CSP Working

Basic CSP cycle during working with HTF and TES is represented in figure 1. During the day HTF is circulated through pipes from collector to storage tanks. The fluid is heated by concentrating solar energy on pipes and heating the HTF to a very high temperature up to 550°C depending upon the design of CSP. Then a part of the HTF is transferred to thermal storage tanks

where it is stored. Mostly the tanks store molten salt at atmospheric pressure. Remaining HTF flows through heat exchanger to heat water and convert it to steam to feed the steam turbine. Steam turbines are coupled to generators which produce electricity. The cycle after converting water to steam is similar to the standard Rankine cycle only replacing burning of fossil fuels to heat water. When electricity is required during night times, hot molten salt from storage tank is pumped through heat exchanger to produce superheated steam, which is then used to drive steam turbines. Hence HTF and TES of molten salt allows power plant to function just as a conventional power plant and does not produce any harmful gases or hazardous material.

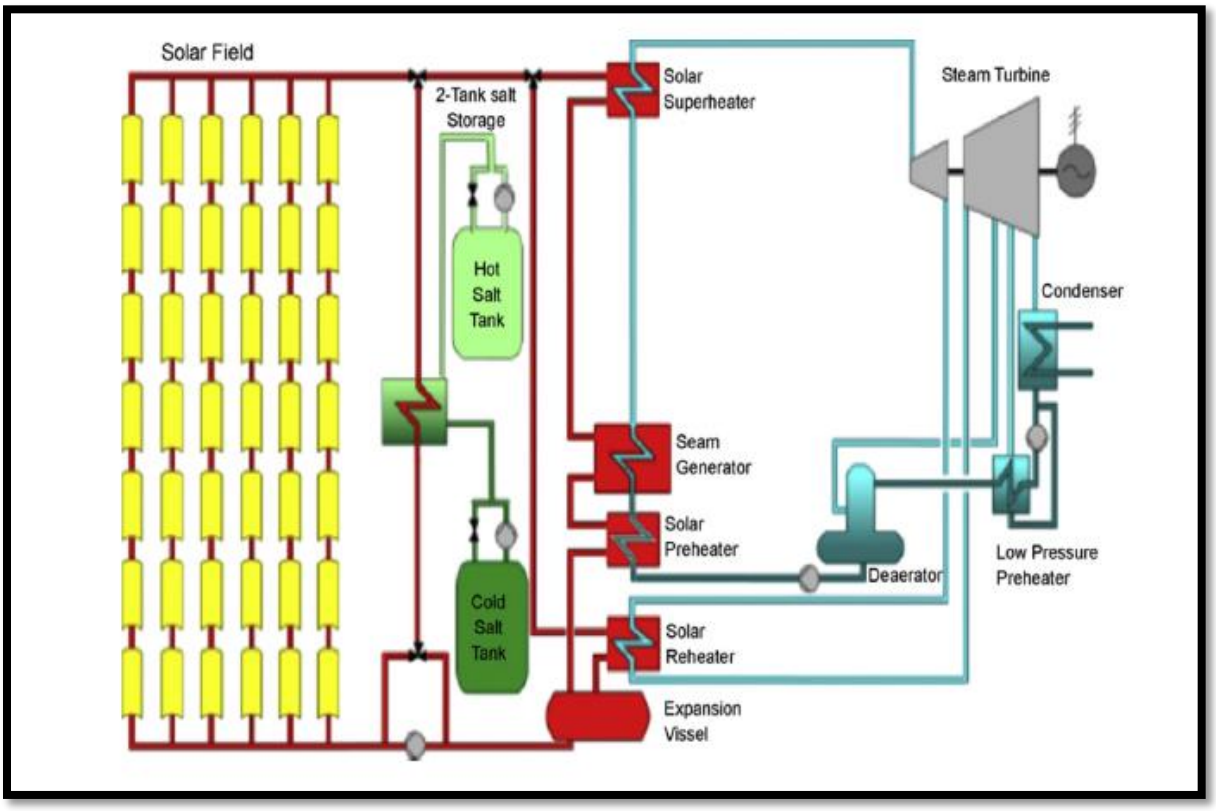

Figure 1: Typical Concentrated Solar Power Plant Using Parabolic Trough Technology [3]

1.3.2 Thermal Energy Storage (TES).

The major technological obstacle for using solar energy is the intermittent nature of the source. This obstacle leads to the requirement of storage of thermal energy for continuous operation which makes the system complex and expensive. Hence it is necessary to use a TES system which is efficient. Economical storage of thermal energy is necessary in CSP plants. Thermal energy can be stored either as sensible heat or latent heat [4]. The total heat storage Q_T by the material is given by-

$$Q_T = m\,[\int_{T1}^{T} c_p\,dT + \Delta H_f + \int_{T}^{T2} c_{pf}\,dT] \quad (1)$$

where,

c_{ps} = solid state Cp value

c_{pf} = fluid state Cp value

H_f = latent heat of fusion

m= mass of storage [4].

Thermal energy storage can be achieved by solids but can be used only for medium temperature. In some solar power plants, liquids are used as a storage material. In some cases sensible heat storage systems use a mixture of rocks and heat transfer fluid like therminol. Latent heat thermal energy storage systems (LHTES) use solid to liquid phase change materials (PCMs). The sensible heat of liquid and / or solid phase can also be used in addition. Latent heat thermal energy storage systems can be effectively used at high temperatures. As the latent heat of fusion is increases, the size of storage system is reduced [4].

Materials used for latent heat thermal energy systems must have high thermal conductivity and high latent heat. They should be non-toxic, non-corrosive, low cost and having

low melting temperature so as to effectively use in CSP plants. Some categories of different materials for thermal energy storage are provided below [4].

Pure materials like lithium fluoride (LiF), lithium hydroxide (LiOH) etc. have high heat of melting but they are expensive. All salts have good thermal conductivities. The commonly used materials are paraffin waxes, fatty acids, metal alloys, salts (fluorides, chlorides, hydroxides, nitrates and carbonates).

Binary systems have better suited melting points and can be combination of expensive material with good storage properties and inexpensive materials. Binary eutectic salts melt and freeze like homogeneous pure substance. This condition occurs when the composition is either eutectic or dystectic. Eutectic composition is represented by the lowest melting point. Dystectic composition creates a mixing phase. A chemical compound and hence behaves almost like a pure substance. Ternary mixtures are eutectic mixtures of three or more materials. The data is available for many ternary and binary eutectics [4].

1.3.3 Heat Transfer Fluid.

The other important parameter to be considered is fluid which will be used for collecting and transferring heat from sun or the heat transfer fluid (HTF). Current practices show use of synthetic oils for heat transfer because of low melting points and high specific heat capacity (c_p) values. Salts are proven to be a good medium for TES but not very viable for HTF. A comparison between salts and oils are shown in table 1. Major properties which are essential for a fluid to be a good HTF are compared [5].

Table 1: Comparison of Important Properties of Current HTF [5].

Thermal Properties and Economics	Units	Solar Salt	Therminol VP-1
Freezing point	°C	220	13
Specific Heat Capacity	J/g-K	~1.550	2.319
Upper Operating Temperature	°C	~580	400
Plant efficiency	%	>40%	10-25%
Storage cost	$/kWh	5.8	57.5
Cost per Kg	$	0.49	3.96

Table 1 is able to clearly highlight properties of synthetic oil which are favorable over solar salt for application as HTF and TES. The freezing point of solar salt being 220°C makes it essential for the entire plant to be always running at more than 220°C as we need to keep the salt in liquid state. Hence a lot of resources are used by the plant itself to keep it at this temperature whereas synthetic oil's freezing point is so low that it will be in liquid state at room temperature and doesn't require any extra resources. Similarly the specific heat capacity of synthetic oil is much higher than solar salt and hence it is bound to give better overall efficiency.

But along with this drawbacks, it is important to note the values from other parameters. The higher operating temperature of solar salt allows it to increase the overall carnot cycle efficiency to about 40% as compared to 10-25% for synthetic oil and physical size of storage is reduced drastically [6]. The storage cost and cost per Kg for solar salt is very less as compared to synthetic oil. To conclude, apart from specific heat capacity and freezing point all other parameters are favorable for solar salt to be used as substitute to synthetic oil as HTF and TES. This observation is further addressed in the thesis objective section.

1.4 Overview of Significant Thermophysical Properties for Application in HTF and TES.

1.4.1 Specific Heat Capacity

Specific heat is defined as the energy required to increase the temperature of a unit mass of a substance by one degree. The energy required for rise in temperature will depend on how the process is carried out. There are two types of specific heats, specific heat at constant volume c_v and specific heat at constant pressure c_p. Specific heat at constant volume (c_v) is the amount of energy required to raise the temperature of the unit mass of substance by one degree, keeping the volume constant during the process. Similarly if we keep pressure constant during the process it is known as specific heat at constant pressure c_p. The value of c_p is always greater than c_v, because at constant pressure system may expand, which will consume some amount of energy [7].

For energy supplied to a fixed mass in stationary closed system undergoing a constant volume process, the change in volume is zero (dv=0). Therefore compression or expansion work is zero. Therefore total energy supplied is utilized in increasing internal energy. Hence at constant volume,

$$du = c_v\, dT \tag{2}$$

$$c_v = (\delta u/\delta T)v \tag{3}$$

When the process is constant pressure process the energy supplied increases enthalpy. Hence at constant pressure,

$$dh = du + pdv \tag{4}$$

$$c_p = (\delta h/\delta T)p \tag{5}$$

From equation (3) and (5), c_p and c_v are expressed in terms of property functions and thus are independent of type of process. Values of c_p and c_v are different at different temperatures and pressures, but the difference is not very large. c_v is related to changes in internal energy and c_p is related to changes in enthalpy. Solids and liquids are assumed to be incompressible substances. Therefore c_v and c_p values of solids and liquids are almost identical and denoted by 'C' [7].

$$c_p = c_v = C \tag{6}$$

The specific heats of incompressible substances depend upon temperature only therefore partial differentials can be replaced by ordinary differential. Hence equation becomes,

$$dh = c_p\, dT = C(T)dT \tag{7}$$

Where,

$$dh = \Delta h = h2 - h1 = \int_1^2 C(T)\, dT \tag{8}$$

The variation in specific heat 'C' with temperature, for a small temperature change, is considered to be linear and the value of C_{avg} is used [7]. It is given by,

$$\Delta h \cong Cav\,(T2 - T1)\ (kJ/kg) \tag{9}$$

For constant pressure and volume,

$$\Delta h = \Delta Q \tag{10}$$

For ideal gas,

$$c_p = c_v + R \tag{11}$$

$$c_p / c_v = K \tag{12}$$

'K' is the specific heat ratio. But for truly incompressible substances two specific heats are same. For solid and liquids (nearly compressible substances) the difference between two specific heats is very small and is usually neglected. The unit of specific heat is kJ/kg^{0}C or kJ/kg K. Instead of

mass, specific heats can be expressed in terms of per mole quantity of material, denoted as $\overline{c}_v$ and $\overline{c}_p$. The unit of molar specific heat is kJ/kmol^{0}C or kJ/kmol K. The product of mass and specific heat of a substance is called as heat capacity. The unit of heat capacity is kJ/ °C or kJ/ K [8].

1.4.2 Latent Heat of Fusion

Large amount of energy is required to melt a solid into liquid or vaporize liquid into gas. The amount of energy absorbed or released during the change of phase is called as the Latent Heat. The amount of energy absorbed during solid to liquid phase change (melting) is called latent heat of fusion. The same amount of heat is released when phase changes from liquid to solid (Freezing) [7].

Similarly the amount of energy absorbed during liquid to gas phase change (vaporization) is called the latent heat of vaporization. The same amount of heat is released when phase changes from gas to liquid (condensation). The value of latent heat is dependent on temperature or pressure at which the phase change process takes place. During this process temperature and pressure are dependent properties. There exists a definite relation between them for the given substance which mathematically can be expressed as

$$Tsat = f\,(Psat) \tag{14}$$

where,

T_{sat} = saturation temperature and

P_{sat} = saturation pressure.

The plot of T_{sat} versus P_{sat} is the characteristic of given pure substance and is called a liquid – vapor saturation curve. The unit of latent heat is kJ/kg. [7]. During the phase change the

temperature remains constant. The amount of heat needed to melt a solid of mass ‘m’ kg may be given by

$$Q = mL\ (kJ) \tag{15}$$

Where,

L= specific latent heat of fusion (kJ/kg) [9]

1.4.3 Freezing Point and Melting Point.

As temperature of liquid is decreased kinetic energy of molecules goes on decreasing. At a particular stage the intermolecular forces become strong and motion of molecules is reduced to minimum value. Liquid molecules start converting into crystals and begin to freeze. The formation of solid state begins at this stage. The temperature at which the phenomenon of solidification takes place is called freezing temperature. At this condition vapor pressure of liquid and solid are equal. Therefore freezing point can be defined as the temperature at which the vapor pressure of liquid is equal to vapor pressure of solid. Similarly when heat energy is supplied to molecules in solid state and they acquire sufficient energy to move away from their fixed position in the matter, there is formation of liquid phase. The temperature at which metal converts to liquid phase is known as melting temperature. At melting point temperature the solid and liquid forms of substance exists at equilibrium, that is solid and liquid phase have equal vapor pressure [10]

The melting point is considered as a characteristics property of substance but some substances can be super cooled beyond the freezing point and therefore freezing point is not considered as a characteristic property of the substance. Most pure substances have same melting

and freezing point but for mixtures and organic compounds, the freezing point is lower than melting point. [10]

1.5 Molten Salts

Molten salt is a mixture of Sodium nitrate 60% $NaNO_3$ and 40% KNO_3 Potassium Nitrate (by weight). Favorable properties of molten salt are that is non-flammable, non-toxic and inert. It has relatively high co-efficient of heat transfer and high density. It can operate at low pressure. Its melting point is ~221°C and freezing point is ~238°C. Molten salt is used as TES and HTF. Compared to other large scale thermal energy storage medium, molten salt is most flexible, efficient and cost effective. In CSP plants, when molten salt is used the backup fossil fuel is not needed. Molten salts can be used up to more than 30 years without replacing. Molten salt can be used as a fertilizer after removing from the plant [11].

Some researchers have tried to find eutectic concentration of mixture of molten salt for $NaNO_3$ and KNO_3 combination. Eutectic point gives the lowest possible freezing point for the mixture. Figure 2 shows phase diagram of different concentrations of $NaNO_3$ and KNO_3. It is observed that close to 50% $NaNO_3$ and 50% KNO_3 combination the eutectic point is observed. [11]. Solar salt of 60% $NaNO_3$ and 40% KNO_3 is preferred over the eutectic mixture as it is a cheaper composition and more stable. Also there is very small difference between freezing points of eutectic mixture and 60%-40% combination which is used in this work.

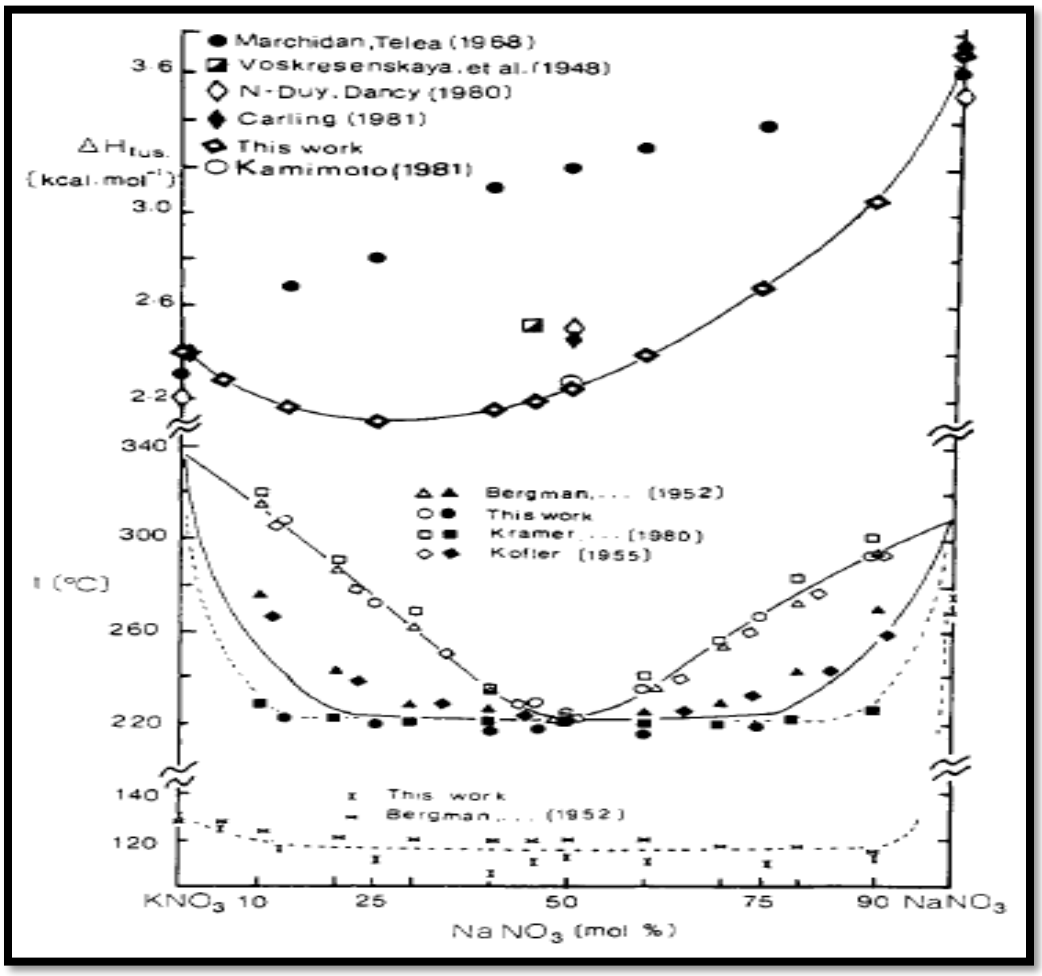

Figure 2: Phase Diagram for $NaNO_3$ and KNO_3 [11]

CSP plant using Molten Salt as HTF and TES offers a realistic solution to the need of generating reliable and emission-free electric power, round the clock. It is a most promising alternative to fossil fuel power plants. But it is necessary to make CSP more efficient and construction cost needs to be reduced. This requirement has initiated lot of research around the world to find solution in above problem area. Earlier it was found that if microscopic particles of material are added to molten salt, its thermodynamic properties can be improved. This lead to a

new research area of adding nanoparticles to molten salt and studying its impact on thermodynamic properties of molten salt [12].

Some drawbacks of molten salts for use in CSP Plants as HTF and TES are poor thermal properties, low energy storage density and corrosion problems [13].

Also High freezing point of molten salt may result in its solidification on a cloudy day or at night. [14] Molten salts exhibits poor heat transfer performance resulting in which cause non uniform heating and laminarization phenomena. Molten salt normally exhibit low thermal conductivity. An easy and cost effective way to improve upon this drawback is to dope them with nanoparticles. [13].

1.6 Nanoparticles and Nanofluids

Nanoparticle is a microscopic particle having at least one dimension less than 100 nm. The properties exhibited by materials change when the size of material particle becomes less than 100 nm. As the size of material becomes less than 100 nm the percentage of atoms at the surface of material becomes significant. The surface area to volume ratio is very high. This changes the properties of material at nanoscale. The behavior of nanomaterials is different because of quantum size effect. When the dimension of material approaches the electron wavelength in one or more dimension, the quantum mechanical characteristics of the electron contribute to change in physical properties of the material [15].

The other reason for different behavior of nanomaterial is due to surface effect. As the nanocrystal size reduces from 30 to 3 nm the number of atoms on its surface increase from 5% to 50%. The atoms at the surface are less stabilized. The origin of quantum size effect mainly

depends upon the type of bonding in the crystal of nanomaterial. Nanoparticles exhibit different properties. For example copper nanoparticles smaller than 50 nm are super hard materials while copper is ductile and malleable [15].

Nanofluids are fluids containing nanoparticles. The addition of nanoparticles to the base fluid forms a colloidal suspension. Nanoparticles used in nanofluids are generally made of metals, oxides of carbides. Common base fluids are water, ethylene, glycol and oil. Large surface to volume ratio reduces specific heat of nanoparticles. Nanofluids containing nanoparticles exhibit enhanced thermal conductivity compared to the base fluid. Though the changes in properties are not always desirable but the above changes are beneficial for our application in molten salts [15].

The thermodynamic properties of molten salts can be improved by adding nanoparticles. A lot of research is presently going on in this area. Type and concentration of nanoparticles for giving most desirable results is being sought after. Several nanofluids have shown increase in effective thermal conductivity. For example –Thermal conductivity of ethylene glycol (EG) was increased by 40% when doped with copper nanoparticles (0.3% concentration by volume). When doped with (4% concentration by volume) copper oxide nanoparticles the thermal conductivity was enhanced by 20%. When oil (poly – alpha – olefin / PAO) was doped with Carbon nanotubes (1% concentration by volume) the thermal conductivity was increased by 150% [6].

1.7 Specific Heat Capacity of Mixture

For combination of MS and NP, the theoretical law of mixture can be applied to find c_p of the mixture. Weight fraction approximation for liquid states is given by,

$$c_{p,nf} = w_{bf} * c_{p,bf} + w_{np} * c_{p,np} \quad (16)$$

where,

$c_{p,nf}$ is specific heat capacity of the mixture.

$c_{p,bf}$ and $c_{p,np}$ are specific heat capacity of MS (1.55 J/gK) and NP (0.88 J/gK).

w_{bf} and w_{np} are weight fractions of MS and NP [16].

Graphical representation of above equation for various combinations of NP and MS is given in figure 3.

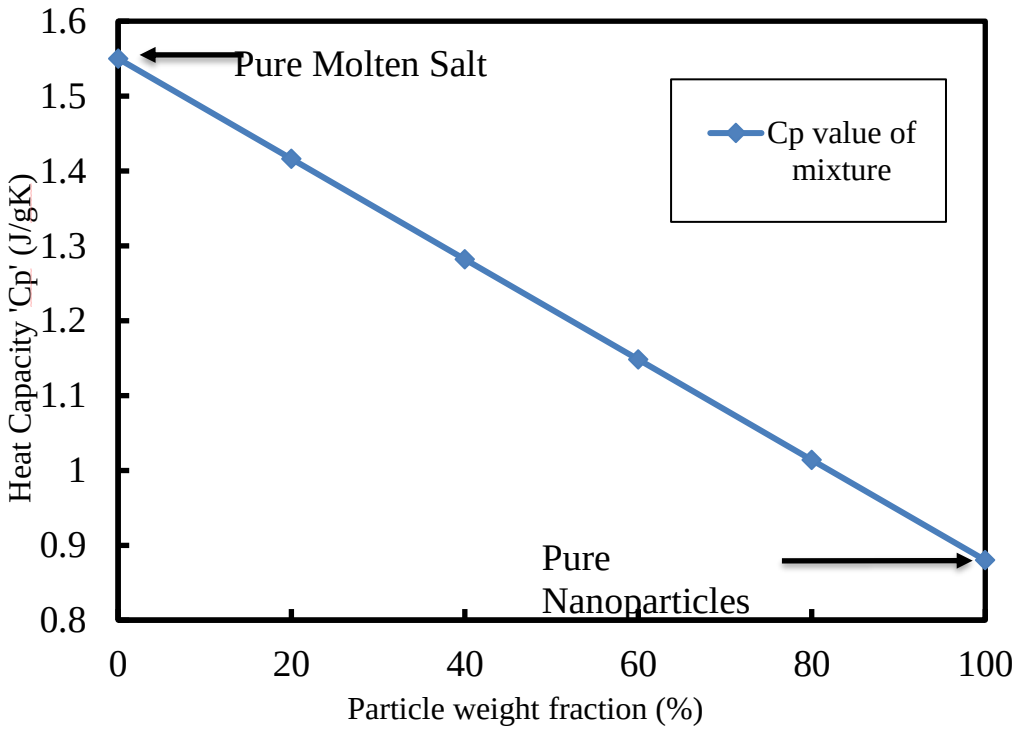

Figure 3: Graph of c_p of Mixture for Various Combinations

As the c_p value of NP is less than that of molten salt, it can be observed that addition of nanoparticles will reduce c_p value of molten salt. But research shows variation in results and surely doesn't align this theoretical model. This has been discussed in further detail in literature review section.

Chapter 2

THESIS OBJECTIVE

2.1 Literature Review

The molten salts are showing tremendous scope for application in CSP and lot of research is being done in this field. This research ranges from testing various types of molten salts and NP to study and enhance various thermal and heat transfer properties. Our research focusses on 60% $NaNO_3$ and 40% KNO_3 combination of molten salt and Table 2 shows specific heat capacity values of this combination of molten salts found by various researchers. Many researchers have shown specific heat capacity values for separately for solid and liquid phase and there is distinctive difference between these values. Important point to note from table 2 is that all researchers have arrived to different values of c_p and uncertainty associated with experimentation methods and instruments used can be accounted for this error.

Table 2: Current Research in Molten Salts

References	**Specific Heat Capacity of MS – Solid ($J \cdot g^{-1} \cdot K^{-1}$)**	**Specific Heat Capacity of MS – Liquid ($J \cdot g^{-1} \cdot K^{-1}$)**
Andreu-Cabedo, et al. [13]	–	1.48 ± 0.09
Chieruzzi, et al. [12]	1.604	1.648
Dudda and Shin [6]	1.21 ± 0.02	1.47 ± 0.02
Lu and Huang [17]	–	1.60
Rogers and Janz [11]	–	1.55
Zavoico [18]	–	1.50
Average	1.407	1.55

Some researchers have tried mixing NP with molten salts, but very few have looked at the effect for combination which is being used in this work. Chieruzzi, et al. has observed enhancement as high as 57.7% by addition of 1% by weight of $SiO_2 – Al_2O_3$ hybrid nanofluid to solar salt in specific heat capacity value. Her results show increment for some combinations and decrement for some. She has studied effect of various types of NP namely, SiO_2, Al_2O_3 and TiO_2. The author has also studied effect of NP addition on heat of fusion, onset temperature and melting temperature for all the combinations mentioned above. The particular combination of 1% by weight of $SiO_2 – Al_2O_3$ has shown reduction in onset and melting temperatures and increase in heat of fusion which are very desirable for application in CSP. These results contradict the theoretical model of law of mixture which suggests that the c_p value of mixture should reduce as NP have less c_p value as compared with molten salt. SEM was also carried to study dispersion of NP in molten salt mixture [12].

Table 3 gives a summary of research done for finding enhancement in thermophysical properties of molten salt based nanofluids. Andreu-Cabedo et al. (2014) has done similar work and found maximum enhancement of 25.03% by addition of 0.5% SiO_2 to solar salt and increment of under 5% for remaining combinations varying from 0.5% to 2.0%. The author has also carried out TGA analysis to find changes in decomposition temperatures of mixture. SEM has been carried out find average sizes of NP and their distribution in mixture [13].

Table 3: Literature Review of MS and NP Nanofluid

Reference	Base Salt	Nanoparticles	Concentration	c_p % change	FP, MP Change
Lu and Huang (2013) [17]	$NaNO_3$ (60%) + KNO_3 (40%)	Al_2O_3 (13 nm, 90 nm),	0.9% to 4.6% wt.	c_p: −10% for 4.6% wt	-
Dudda and Shin (2013) [6]	$NaNO_3$ (60%) + KNO_3 (40%)	SiO_2 (5 nm, 10 nm, 30 nm, 60 nm),	1% wt	c_p: +10% (5 nm) +13%, (10 nm), +21%(30 nm), +28% (60 nm)	-
Chieruzzi et al. (2013) [12]	$NaNO_3$ (60%) + KNO_3 (40%)	SiO_2 (7 nm), Al_2O_3 (13 nm), TiO_2 (20 nm), SiO_2+ Al_2O_3 (2 to 200 nm)	0.5% to 1.5% wt.	+19.9% (Al_2O_3) -14.4% (TiO_2) +57.7% (SiO_2+ Al_2O_3)	MP -10°C, FP -9°C, ΔH +17.2 J/g
Cabedo et. al., (2014) [13]	$NaNO_3$ (60%) + KNO_3 (40%)	SiO_2 (12 nm),	0.5% to 2.0% wt.	c_p: +25% (1.0% wt.)	-
Ho and Pan (2014) [9]	$NaNO_3$ (7%) + KNO_3 (53%) + NaNO2 (40%)	Al_2O_3 (<50 nm),	0.016% to 1% wt.	c_p: +19.9% (0.063% wt.)	-
Lu – di Zhang et. al (2016) [19]	KNO_3 – $NaNO_3$ - $LiNO_3$ – $Ca(NO_3)_2$, $4H_2O$, (6 : 1 : 2 : 2 in mass ratio)	SiO_2 , 20nm size	1% wt	c_p: +21.2%.	-
Shin and Banarjee (2013) [20]	Li2CO3 (62%) + K2CO3 (38%)	SiO_2 (2 to 20 nm),	1% wt.	c_p: +124% (zone type A), c_p: +0% (zone type B)	-

Lu and Huang (2013) have reported somewhat contrasting results to Andreu-Cabedo et al. and Chieruzzi, et al. Lu and Huang have shown reduction in specific heat capacity values by adding different concentrations of alumina NP. They have also studied effect of changing size of NP and have found similar trend of reduction in c_p values. SEM images depict the morphological characterization of the mixture and dispersion of NP.

Researchers like Dudda and Shin (2012), Ho and Pan (2013) and Zhang et al. (2016) have done similar research but with different molten salts and various types of NP. Dudda and Shin (2012) has shown increase in specific heat whereas Ho and Pan (2013) and Zhang et al. (2016) have shown increase in c_p value for some concentration of NP while decrease for some concentrations. c_p value calculations by far has been done on a DSC and morphological analysis using SEM.

2.2 Thesis Objective and Scope.

2.2.1 Thesis Objective

With reference to table 1, we concluded that lower specific heat capacity and high freezing point of solar salt are two major arguments which don't support the replacement of synthetic oil with solar salt as HTF and TES system. Main objective of this thesis is to investigate changes in specific heat capacity, freezing point, melting point and enthalpy of fusion of solar salt on adding nanoparticles.

Along with investigating changes in thermophysical properties, changes in microstructure need to be analyzed to estimate dispersion of NP and also check for any changes in structure of solar salt and NP due to mixing. Enhancement in thermophysical properties will eventually further argument of using MS as HTF and TES in CSP.

2.2.2 Thesis Scope

Based on above literature review, there is lot of ambiguity over the exact effect of addition of nanoparticles in molten salts. As seen earlier, there are different research showing increase and decrease in specific heat capacity of different kinds of molten salt on addition of nanoparticles. There is a need to predict a model which will be in line with the anomalous of molten salts nanofluid mixture and will be able to predict the specific heat capacity values for various concentrations. Since there are many salts whose combination is referred to as molten salt, we will be restricting our study and experimentation to 60% $NaNO_3$ and 40% KNO_3 by weight combination, typically called as solar salt.

One of the important factor while considering addition of nanoparticles, is the type of nanoparticles. Since there are many types of nanoparticles available based on different materials, the thesis will focus on effect of adding a combination of nanoparticles to solar salt. Aluminum oxide and titanium oxide nanoparticles will be added to solar salt to classify the mixture as hybrid nanofluid (Al_2O_3 and TiO_2). Effect of varying concentration of these nanoparticles, as per table 4 will be discussed in later sections.

Table 4: Combination of Al_2O_3 and TiO_2 in Different Quantities.

Sr. No.	**Type and quantity of nanoparticle 1**	**Type and quantity of nanoparticle 2**
1	Al_2O_3 – 100%	TiO_2 – 0%
2	Al_2O_3 - 75%	TiO_2 – 25%
3	Al_2O_3 – 50%	TiO_2 – 50%
4	Al_2O_3 – 25%	TiO_2 – 75%
5	Al_2O_3 – 0%	TiO_2 – 100%

Variation in concentration of nanoparticles when mixed with solar salt will be of prime importance. This variation will be for 0%, 0.5%, 1%, 2.5% and 5% by volume for above combinations. The volume to weight conversion is done with basic density and volume conversions. A MATLAB code to assist in same is prepared and attached in appendix.

The freezing point, melting point and latent heat of fusion will be also be calculated for all the samples. The changes in these will be discussed as compared to solar salt with no NP. DSC will be used to calculate thermophysical characteristics and SEM to study morphological characteristics. Uncertainty analysis of these values will be done to predict error in calculations and experiments.

Chapter 3

MOLTEN SALT AND NANOPARTICLE NANOFLUID

3.1 Details of Material Used

3.1.1 Molten Salt

Molten salt consisting of 60% $NaNO_3$ and 40% KNO_3 is manufactured in house. Raw material for manufacturing molten salt i.e. $NaNO_3$ and KNO_3 were purchased from Sigma Aldrich possessing of 99.9% purity. Glove box is used to store salts and prevent exposure to atmosphere. For our manufacturing process, the last step consists of melting salt and evaporating moisture from the mixture. So technically the glove box doesn't play a huge role in preventing exposure to moisture but it is a good practice to store salts in glove box.

3.1.2 Nanoparticles

Nanoparticles were purchased from US Research Nanomaterials Inc. The hybrid nanofluid consists of aluminum oxide and titanium oxide nanoparticles. While purchasing, it is important to consider parameters like size and phase of nanoparticles. For aluminum oxide, 'α' phase nanoparticles of 80 nm size are being used. The 'α' phase is considered as a more stable phase of alumina as it is produced during last stage of manufacturing at high temperature [21]. The titanium oxide particles are of 'rutile' phase and 100 nm in size. The size selection is done to be consistent with sizes of alumina and titanium oxide particles. The size of nanoparticles has ability to affect thermal properties and hence it is a good practice to be consistent with size for

both types of nanoparticles. Sizes of nanoparticles available vary from 5 nm to 300 nm. Similarly various phases like ‘α’, ‘β’, ‘γ’ and ‘θ’ are available for alumina and ‘rutile’, ‘anatase’ and ‘brookite’ are available for titanium oxide [21]. Deionized water is used to add to mixture and then evaporate to melt molten salt mixture. Some additional properties for aluminum and titanium oxide provided by manufacturer are collected in table 5 and table 6 respectively.

Table 5: Properties of Alumina NP [22]

Aluminum Oxide Nanoparticles (100% alpha)	**Description**
Al_2O_3 Nanoparticles Purity:	99+%
Al_2O_3 Nanoparticles APS:	80 nm
Al_2O_3 Nanoparticles Grain Size:	27 nm
Al_2O_3 Nanoparticles SSA:	>15 m^2/g
Al_2O_3 Nanoparticles Morphology:	Nearly spherical
Al_2O_3 Nanoparticles Color:	White
Al_2O_3 Nanoparticles Density:	3.97 g/cm^3
Al_2O_3 Nanoparticles Crystallographic Structure:	Rhombohedral

Table 6: Properties of Titanium Oxide NP [22]

Titanium Oxide Nanoparticles (100% rutile)	**Description**
TiO_2 Nanoparticles Purity:	99.9+%
TiO_2 Nanoparticles APS:	100 nm
TiO_2 Nanoparticles SSA:	~15-35m2/g
TiO_2 Nanoparticles Color:	White
TiO_2 Nanoparticles Morphology:	Near spherical
TiO_2 Nanoparticles True Density:	4.23 g/cm3

3.2 Details of Instruments Used

Glove box or controlled environment chamber used to store nitrate salts was purchased from Electro-tech Systems Inc. with model no. 5503-00 package A. Digital analytical balance USS-DBS5 of US Solid lab equipment was used for weighing sample and nanoparticle mass. Branson-1800 sonicator was used for sonication of nanofluid. DSC was used to perform analysis and testing of nanofluid to determine thermophysical properties. DSC is a Perkin Elmer DSC7 with Thermal Analysis Controller TAC 7/DX used for heating and temperature control of samples. Aluminum pans of approximately 15 mg were used for holding samples in DSC. The DSC comes with Pyris software which used for thermal analysis and obtaining data. The SEM used for morphological analysis was Joel JSM-7500F field emission SEM. The SEM was present at Argonne national lab and we thank them for allowing us to access the services of SEM. Glass vials and beakers were used for storing and preparing samples Figure 4 gives a flowchart of the entire process from preparation to analysis.

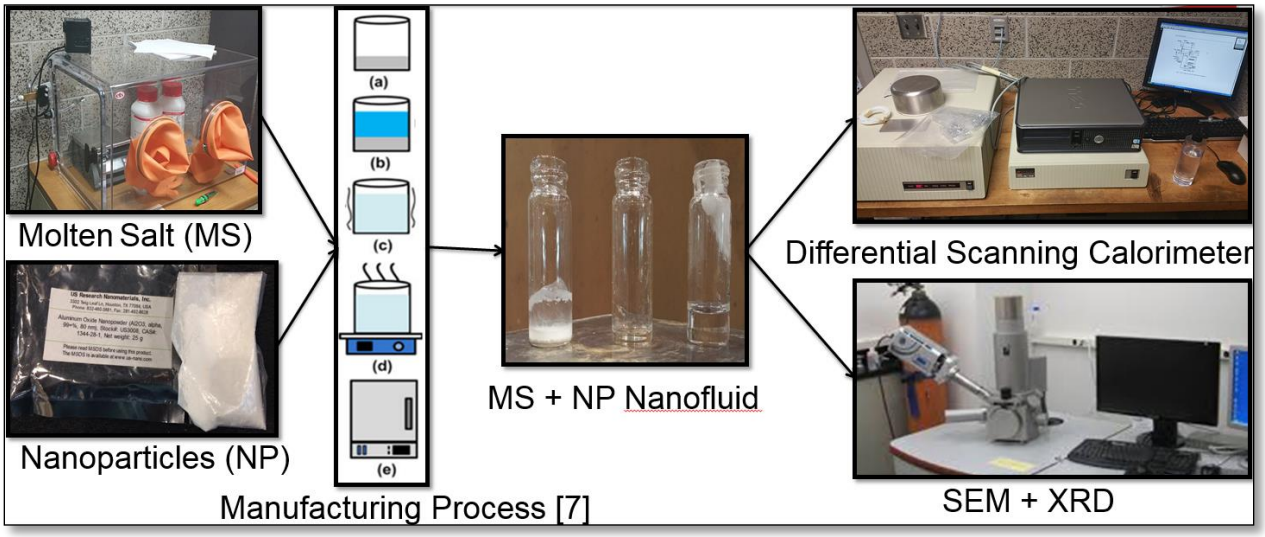

Figure 4: Flow Chart for Experimental Synthesis and Testing

3.3 Experimental Methodology

The synthesis of nanofluids was carried by adding different concentrations of alumina and titanium oxide nanoparticles into solar salt (i.e. molten salt with 60% $NaNO_3$ and 40% KNO_3). Alumina nanoparticles ('α' phase Al_2O_3 particles, 80 nm size) and titanium oxide nanoparticles ('rutile' phase, 100 nm size) were bought from US Nanomaterials Research Inc. while $NaNO_3$ and KNO_3 salts were bought from Sigma Aldrich. The method used for synthesis is similar to the one adopted by Lu and Huang [17]. Different concentrations of alumina and titanium oxide nanoparticles were measured by volumetric fractions. Wide range of concentrations ranging from 0.5% to 10% by volume were used to obtain relations between concentrations and heat capacity. These volumetric concentrations of NP were converted into weight fractions and then added to beaker consisting of a mixture of 60% by weight of $NaNO_3$ and 40% by weight of KNO_3 in solid state. MATLAB code based on basic density calculations for converting from percent volume to percent mass is attached in appendix. Total sample prepared for each batch was 5 gm (a). De-ionized water by ratio of 1:100 was added to beaker (b). This mixture was then sonicated for about 100 mins in ultra-sonic bath (Branson, M1800) (c). After sonication, a homogenous mixture was obtained. The mixture was then heated on hot plate (Fisher Scientific) with a magnetic stirrer (to ensure that NP are not accumulated) at about 170°C for ~55 mins till DI water was evaporated (d). Melting point of solar salt is in range of 220°C. The salt containing NP was then heated in furnace (Omegalux, LMF-3550) at 300°C for 40 mins to achieve complete melting and mixing of both salts (e). The solution was then cooled in atmosphere to obtain white solid mixture. Pure solar salt was prepared in same manner without adding NP. Small samples (~20 mg) of this mixture were then transferred in aluminum pans to be tested in differential scanning calorimeter (Perkin Elmer,

DSC7). These nanofluids were synthesized without use of any surfactant. Experimental procedure is shown in figure 5.

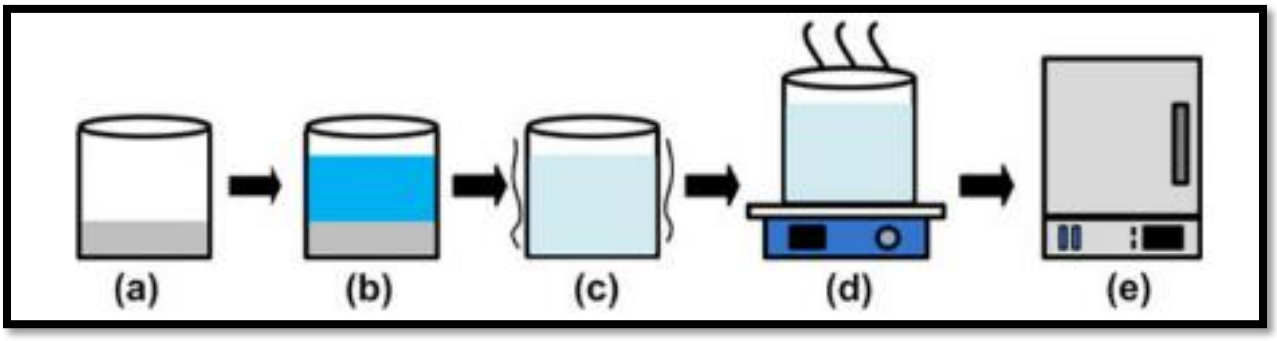

Figure 5: Preparation Method for Molten Salt Nanofluid [17].

This work has total 6 types of samples and each sample has further sub-samples for different concentrations. Table 7 lists different samples and its abbreviations which will be used throughout this work.

Table 7: Abbreviations for Samples Manufactured

Sample Name	**Abbreviation**
Pure Molten Salt	Sample A
Molten Salt with Al_2O_3 NP	Sample B
Molten Salt with 75% Al_2O_3 and 25% TiO_2 NP	Sample C
Molten Salt with 50% Al_2O_3 and 50% TiO_2 NP	Sample D
Molten Salt with 25% Al_2O_3 and 75% TiO_2 NP	Sample E

CHAPTER 4

CHARACTERIZATION

4.1 Morphological Analysis Using Scanning Electron Microscope (SEM)

SEM has been extensively used to study and understand changes in microstructure of the molten salts on addition of nanoparticles. SEM pictures can give a very high magnification of power of few nanometers and hence it is possible to observe changes in microstructure on combining molten salt and nanoparticles. Along with changes in microstructure, it is important to observe dispersion of nanoparticles in nanofluid. The changes in values of different thermophysical properties of molten salts are observed on addition of nanoparticles. With help of SEM images, we can prove that one of the reasons for these changes is dispersion of nanoparticles throughout fluid. Thus using SEM pictures we can further validate dispersion of nanoparticles in molten salt.

The SEM uses an electron beam which is focused with help of electromagnetic coils on sample. The electron signal reflected from the sample is converted to a visual image and obtained on the monitor [23]. The principle of operation of SEM is based on physics of light microscopy. It has been proved that human eye cannot distinguish between 1/60° visual angle at a viewing distance of 25 cm. Using optical lens this resolution was increased to ~2000. Further in SEM, the light source was replaced by high energy electron beam which produced large number of signals based on topography of the specimen [23].

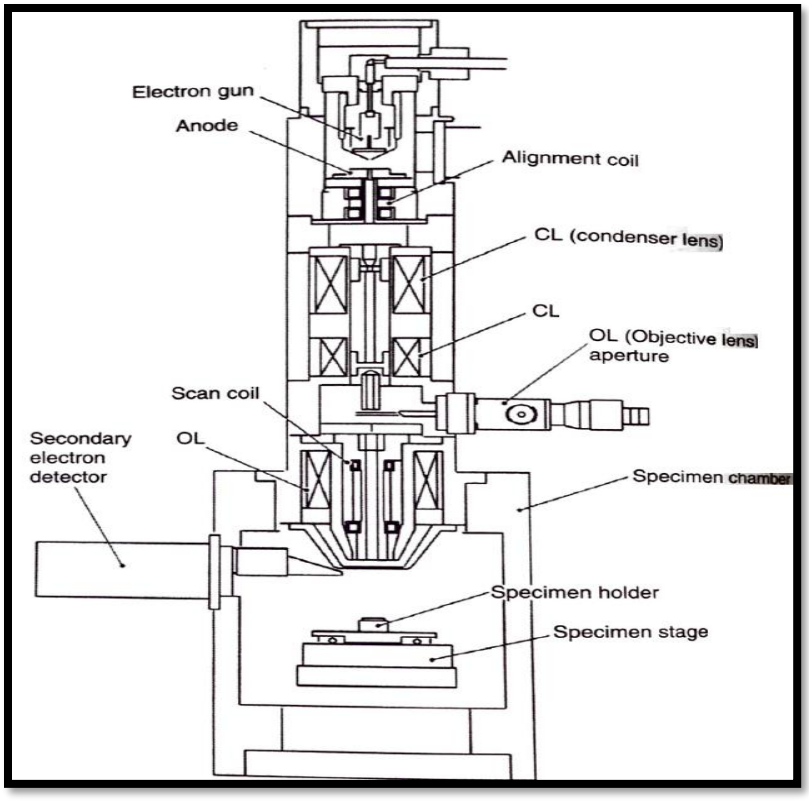

Figure 6: Cross Sectional View of SEM [23]

Figure 6 shows a schematic of standard SEM. The electron gun produces electron beam based on different energy levels from 0.1 to 30 keV. The smaller the diameter of the beam, better the resolution of image obtained. Electromagnetic lenses and apertures are used to focus electron beam from hairpin tungsten filament as it is found to be too large to produce a high resolution image [23]. The image obtained is a reconstruction of specimen obtained by signal emitted from specimen when illuminated by high energy electron beam and is not a true image [24]. Many parameters of SEM needs to be taken into consideration before getting an image of good resolution and magnification. Parameters like energy of electron beam, lens current, working distance (WD) are required to be set to obtain high quality image. Vacuum pump forms an integral part of the assembly. It used to avoid scattering of beam and contamination of electron gun [23].

Figure 7: Joel JSM -7500 F SEM

We have been fortunate to receive access to a world class facility at Argonne National Lab. The SEM we used is a Joel JSM-7500 F field emission SEM. Figure 7 shows the image of Joel make SEM which has been used for this work. Sample preparation requires loading specimen of nanofluid directly on a carbon tape attached on an aluminum plate. The plate was roughly 1in. by 1 in. in size. This plate was then secured on the stage using copper tape. Copper tape acts as gluing agent without grounding it. It is important to check if aluminum plate and grove of the stage flush together as it will distort image. We can use carbon tape to fill the gap. Each stage was loaded with 6 samples. The stage has an arrow engraved on one of its side. It will be useful while locating the samples. For obtaining a good resolution image we have to adjust the working distance and energy level of electron gun. We obtained a good resolution image at 10 keV energy and 10 µA current. We have adjusted the working distance or distance in ‘z’

direction as 4.5 mm. After adjusting these values and orientation of arrow we start focusing the sample. Low magnification mode is used to move around and particular regions on samples. Image of each specimen was captured at different magnification powers. Standardized on three magnification powers namely 10k, 20k and 50k was done. At these magnification power the images were able to magnify to a scale of 100 nanometers. Also images have been taken from different regions of the same specimen to study if there is any difference in the dispersion of nanoparticles in nanofluid. Some images of SEM are attached and discussed below.

4.2 Thermal and Heat Transfer Analysis Using DSC.

The thermophysical properties of molten salt nanofluid are studied using DSC. Thermophysical properties namely specific heat capacity (c_p), melting point, freezing point and latent heat of fusion are being observed in this study. The DSC has two furnace, one for sample and one for reference. The DSC is a calorimeter which measures thermal motion in form of heat flow. This heat flow is converted into heat capacity by repeating the test for an empty pan and reference material. The reference furnace is always kept with an empty pan. Part of heat provided by DSC to heat the sample is used to heat the environment and pan in which sample is kept. Hence all heat provided by DSC is not absorbed by sample. The reference furnace comes into picture to avoid this situation and give accurate value of heat absorbed by the sample. Since reference furnace has an empty pan, it provides the same environment and empty pan as for the sample. Same quantity of heat at same rate is provided to both furnace. While calculating the heat flow, DSC gives difference between two furnaces. This heat flow is equal to heat absorbed by sample only [25].

DSC gives very accurate values of heat absorbed with incremental temperature. The precision is around ± 0.002 mW as per manufacturer's specification.

The program used for DSC has been adopted from Cheiruzzi with some modifications. The sample is first held at 300°C for 15 minutes to evaporate presence of any moisture. The sample is bought to 140°C at rate of 10°C / min and then start the cycle for finding thermal properties. The program starts with holding at 140°C for 3 mins, heating to 300°C at 10°C / min, holding at 300°C for 3 mins and cooling to 140°C at 10°C / min. The same cycle is carried out for 3 times to take care of any errors arising due to repeatability. The modifications from proposal stage was to reduce the starting point from 150°C to 140°C. The reason for this modification is that reference material used for experiment is indium and melting point is 156.6°C. Since it close to the initial start point of 150°C, some cases due to small fluctuation in temperature, the indium starts melting during 150°C hold portion at start of program. Hence the starting point is moved to 140°C. The graph of DSC program representing symmetric temperature changes w.r.t time is shown below.

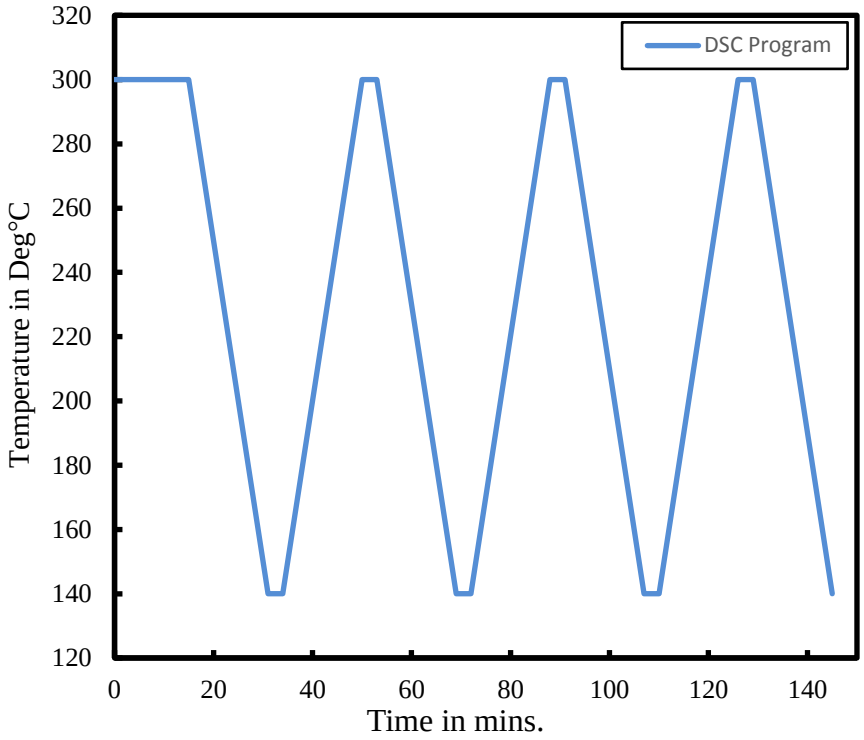

Figure 8: Graph of DSC Program.

The measurement procedure adopted is called as classical three-step DSC procedure [16]. The program explained above is used for two empty pans loaded in DSC. The baseline heat flow with respect to temperature change is observed during this run and denoted by Q_0. The next step is measurement of reference material indium loaded onto one of the empty pan. The indium sample weights are measured using analytical balance and are approximately 20 mg which is denoted by m_{ref} and adheres to ASTM standard requirements. The heat flow values for reference material are obtained as Q_{ref} for same program and $c_{p\ ref}$ is known to be 0.262 J/gK. The third step is loading same pan with molten salt nanofluid after unloading indium material. The same program is run to find Q_{sample} value which is heat flow for particular temperatures. The weight is in range of 20 mg and is measured as m_{sample} [16].

The ASTM standard test method to determine c_p using DSC put forth in E 1269-05 standard has been followed. The $c_{p,\,sample}$ value is calculated by following equation.

$$c_{p\,sample} = \frac{Q_{sample} - Q_0}{Q_{ref} - Q_0} * \frac{m_{ref}}{m_{sample}} * c_{p\,ref} \quad (17)$$

The c_p value for mixture has been calculated for solid phase and liquid phase. A sample calculation has been done to provide more insight into this topic. It is important to understand the temperature range of experimentation which needs to be considered. The test for DSC starts at 140°C. Melting point for molten salt is around 221°C. So the temperature range between 140°C and 221°C can be used to find c_p value of solid phase. But since indium is used as reference material, its melting point is 156.6°C and a phase change along accompanied by curve and peak is observed as represented in Figure 9. This high value will defer the c_p value of sample and hence we need to start calculating from after indium has melted. The start point for $c_{p,solid}$ is taken as 160°C up to onset temperature. $c_{p,liquid}$ is calculated on return cycle i.e. cooling from 300°C to freezing point i.e. around 238°C. Since the program for molten salt has three cycle runs, we get average value at each temperature increment and then total c_p value is calculated as average over the above mentioned ranges for solid and liquid phase respectively.

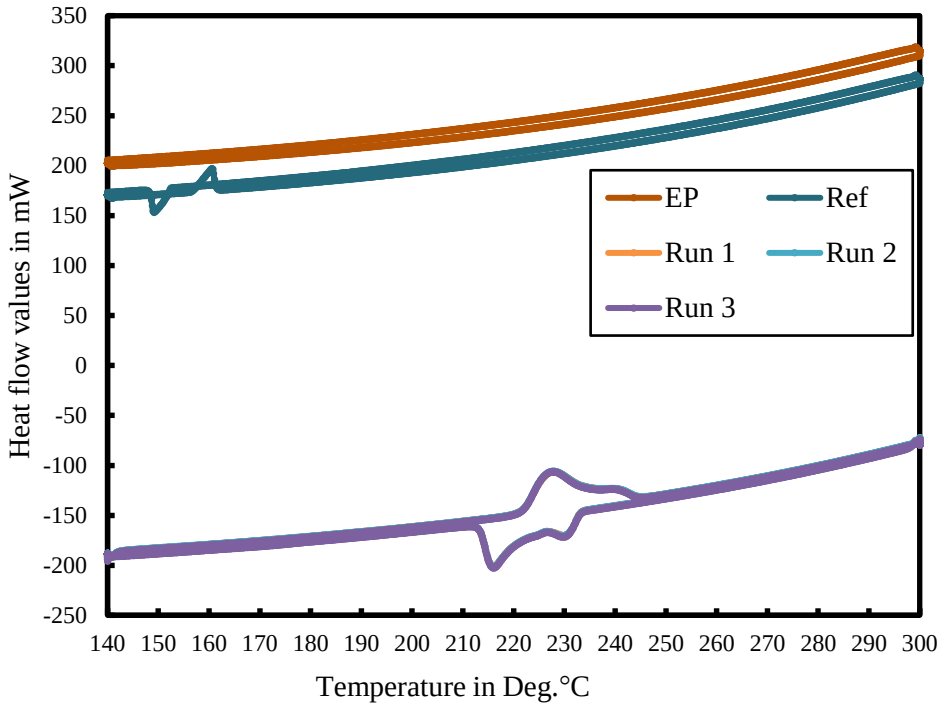

Figure 9: DSC Output Curve for 1% Concentration of 25% Al_2O_3 and 75% TiO_2.

Sample calculation is done in the following section. The above graph shows a DSC output curve for a 1% concentration of 25% Al_2O_3 and 75% TiO_2. Empty pan, reference pan and sample are run separately and hence separate graphs are obtained. The above graph is a combined graph of empty pan, reference pan and sample runs. The X axis shows the heat required to increase temperature from 140°C to 300°C at rate of 10°C / min. The run 1, 2 and 3 are the three cycle runs described above. These three different runs done for sample to account for errors associated with the machine due to repeatability. The graphs overlap each other and are seen as one in above figure and thus show great accuracy of machine. Around 2300 data points are obtained for 1 cycle run. These are imported into Microsoft Excel software for further data cleaning and analysis. This data is then arranged to match heat flow values of empty pan, reference and sample to same temperatures. Thus we obtain a heat flow value for temperature range of 140 to 300°C with increment of approximately 0.167°C.

Consider example of solid phase at temperature of 163.7°C. The heat flow values for empty pan, reference and sample are 207.035, 176.202 and -177.751 mW respectively. Mass of reference and sample for this particular experiment was measure to be 10.9 and 23.3 mg respectively. c_p value of indium reference material is 0.262 kJ/kgK. Substituting these values in equation 17 we obtain c_p value of 1.53 kJ/kgK. Similar calculation can be done for liquid phase during return cycle at any temperature between 300°C and 240°C (freezing point) Hence c_p value is calculated from equation 17 for all these temperatures and average over the range for solid and liquid phase mentioned above is done to arrive at c_p value of sample for a particular phase.

The freezing and melting point calculation is taken at onset temperature [cheiruzzi]. The onset temperature can be compared to glass transition temperature. At glass transition temperature, the sample begins to exhibit liquid properties. At this temperature, there is thermal and transitional motion which begins to set in before sample is entirely converted into liquid form and hence its direct comparison with melting point has been widely accepted [book arl-tr-2413]. The latent heat of fusion values are found out at solid to liquid phase conversion and vice versa. Figure 9 of heat flow vs. temperature for molten salt is obtained from DSC for each run. This graph is for 1% concentration of 25% Al_2O_3 and 75% TiO_2 which is considered for above example. The curve is a constant slope curve when the sample is in one particular state. But for transition, there is a rise in heat flow and peak is observed. This transition period of phase conversion gives latent heat of fusion in J/g. The melting and freezing point calculated at onset temperature are shown in figure 10 and 11. The Pyris software provides these values. For the above example, onset value for solid phase (melting point) is 221.72°C and latent heat of fusion is 115.9691 J/g. Similarly figure 11 gives value for the liquid phase. Freezing point obtained is 233.11°C and latent heat of fusion is -123.9537 J/g. Negative sign for latent heat of fusion

denotes heat lost to change phase from liquid to solid. The changes in freezing, melting point and latent heat of fusion before and after adding nanoparticles are analyzed in sections to follow.

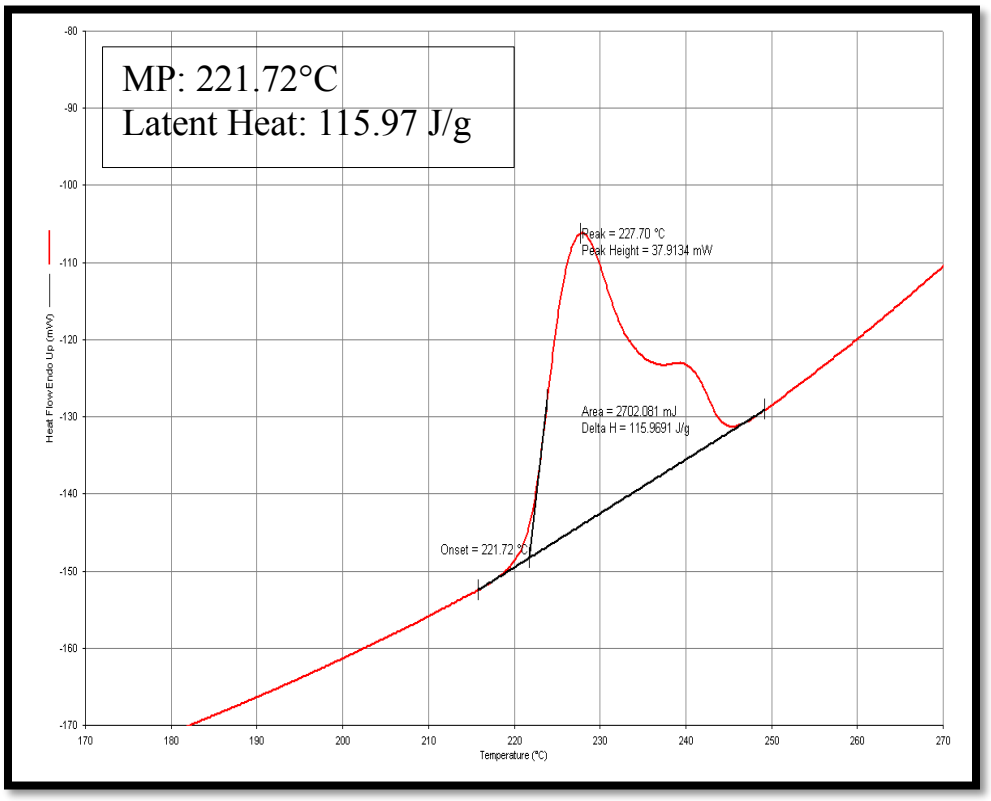

Figure 10: DSC Curve for Solid Phase

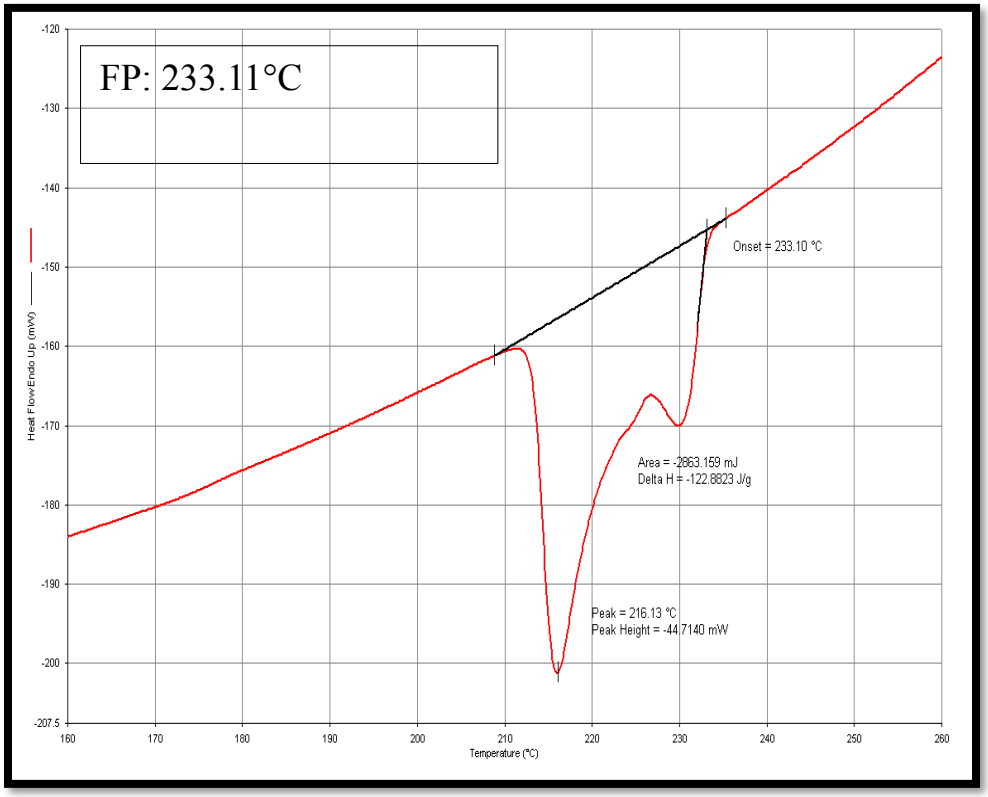

Figure 11: DSC Curve for Liquid Phase

4.3 Uncertainty Analysis and Calculation

One of the major challenges in finding specific heat capacity value (c_p) of different molten salt mixtures is assessing the error associated with the measurement. Since true value of specific heat capacity is not known, it is difficult to estimate the range of error. Based on range of error value, we can determine authenticity of obtained results. These errors arise in each and every step of tests and measurement and thus reduces our ability to find the true value. This numerical error value is called as uncertainty value associated with the measurement. Uncertainty is broadly categorized into systematic (bias) uncertainty and random uncertainty [26]. c_p value is given by,

$$c_p = \bar{c}_p \pm U_{c_p} \tag{18}$$

4.3.1 Systematic Error:

Error obtained in repeated measurement under constant conditions is called as systematic error. Since it does not vary with each measurement, it gives an offset value from true value and affects each measurement equally [27]. Sometimes it becomes difficult to its find value because of its constant nature [26]. Systematic uncertainty for our experiment lies within accuracy of instruments used for testing. Error value associated with DSC and measuring scale is provided by their respective manufacturers. Since our final aim is to find uncertainty associated with specific heat capacity value, we analyze its formula to determine systematic uncertainty. It is given as follows

$$c_{p_{sample}} = \frac{Q_{sample} - Q_0}{Q_{ref} - Q_0} * \frac{m_{ref}}{m_{sample}} * c_{p_{ref}} \quad (19)$$

For our convenience, let us assign $Uc_{p,b}$ as the systematic standard uncertainty. It is over the interval $\pm Uc_{p,b}$. Each interval is assigned over a probability level or confidence level. The systematic error over this confidence level is $t*Uc_{p,b}$ where t represents a precision interval. This precision varies with respect to probability P% which is selected by the user based on his experiments and readings. For our experiment we are choosing 95% probability level. This is based on confidence that 95% of our readings lie in the range of Cp and is a standard widely accepted [26].The systematic uncertainty at 95% probability is given by

$$\pm B = \pm (t * Uc_{p,b}) \ (95\%) \quad (20)$$

Two instruments used for measurement are DSC and weighing scale which have potential to induce systematic error in each sample irrespective of nature of the sample. For DSC, this error can be induced based different aspects like calibration method, thermal lag during heat flow cycle, Noise (RMS) and calorimetric accuracy values can be found from specification sheet provided by manufacturer.

It is as follows:

U_N= 0.002 mW (Noise (RMS) value).

U_{CA}= 1% of reading (Calorimetric Accuracy)

U_{PA}= 0.1% of reading (Calorimetric Precision)

$$U_Q=\sqrt{U_N{}^2+U_{CA}{}^2+U_{CP}{}^2} \tag{21}$$

Where U_Q is total error associated with DSC measurement. Similarly for analytical balance, error associated with measuring each sample is based on least value measured by machine. As per manufacturer, U_{mass}= 3.6 mg. It is important to note here that units of each error are equivalent to measured property.

To find systematic error based on c_p formula, we will partially differentiate c_p value with respect to variables which are measured using DSC and weighing machine. From equation (c_p equation), we can see that on RHS except $c_{p_{ref}}$ term we have to use partial differentiation for each term. The resultant error value will be given by:

$$U_{Cp,b}=\sqrt{\left[\left[\frac{\delta cp}{\delta m_{ref}}*U_{mass}\right]^2\right]+\left[\left[\frac{\delta cp}{\delta m_{sample}}*U_{mass,am}\right]^2\right]+\left[\left[\frac{\delta cp}{\delta Q_{sample}}*U_{Qsample}\right]^2\right]+\left[\left[\frac{\delta cp}{\delta Q_{ref}}*U_{Qref}\right]^2\right]+\left[\left[\frac{\delta cp}{\delta Q_0}*U_{Q_0}\right]^2\right]} \tag{22}$$

where,

$$\frac{\delta cp}{\delta m_{ref}}=\frac{Q_{sample}-Q_0}{Q_{ref}-Q_0}*\frac{1}{m_{sample}}*c_{p_{ref}}$$

$$\frac{\delta cp}{\delta m_{sample}}=-\frac{Q_{sample}-Q_0}{Q_{ref}-Q_0}*\frac{m_{ref}}{(m_{sample})^2}*c_{p_{ref}}$$

$$\frac{\delta cp}{\delta Q_{sample}}=\frac{1}{Q_{ref}-Q_0}*\frac{m_{ref}}{m_{sample}}*c_{p_{ref}}$$

$$\frac{\delta cp}{\delta Q_{ref}}=-\left(\frac{Q_{sample}-Q_0}{(Q_{ref}-Q_0)^2}\right)*\frac{m_{ref}}{m_{sample}}*c_{p_{ref}}$$

$$\frac{\delta cp}{\delta Q_0} = \left(\frac{Q_{sample}-Q_0}{(Q_{ref}-Q_0)^2}\right) * \frac{m_{ref}}{m_{sample}} * c_{p_{ref}}$$

Since, only one weighing machine used for weighing all the samples, $U_{mass}=U_{mass,am} = 3.6$ mg. Similarly for DSC, $U_{Qsample}=U_{Qref}=U_{Q0}=U_Q$. Since each sample has more than 8,700 data points over range of our measurement for MS, we are going to show the calculation for each systematic error in excel sheet.

4.3.2 Random Error:

Variation or scattering of each measurement in a set of repeated measurement from mean value represents random error. The estimate of range of this error is given by random uncertainty and defined by $Uc_{p,r}$. The random standard uncertainty is given by $s_{\bar{x}}$ over the interval $\pm s_{\bar{x}}$ where,

$$s_{\bar{x}}=s_x/\sqrt{N} \quad (23)$$

s_x Stands for sample standard deviation over range of measurement and N is number of measurements or number of repetitions. Sample standard deviation can be found out by following method:

$$s_x=\left(\frac{1}{N-1}\sum_{i=1}^{N}(x_i-\bar{x})^2\right)^{1/2} \quad (24)$$

where $(x_i-\bar{x})^2$ gives the deviation of x_i. The concept of probability level or confidence level is also considered for random uncertainty error. We will consider 95% confidence level for our experiments. Based on this consideration, we can find the total random uncertainty error as follows:

$$\pm R=\pm(s_{\bar{x}} * t_{cp,r}) \quad (95\%) \quad (25)$$

We can use above method of finding random error to find error associated with calculation of c_p value. As mentioned earlier, large number of data points of heat flow are obtained for each sample. Hence we shall carry out these calculations in excel sheet. The total uncertainty will be root mean square of systematic and random error and can be denoted as follows:

$$U_{cp} = \pm\sqrt{B^2 + R^2} \quad (95\%) \tag{26}$$

Substituting this value in equation for c_p, we can establish uncertainty range. The values obtained from this analysis can be compared with the works of Chieruzzi and Lu. From these uncertainty values we can estimate accuracy and range of c_p values in our experiments.

Chapter 5

RESULTS AND DISCUSSION

5.1 SEM Images and Discussion

SEM is used for morphological analysis of nanofluids. Since it has been suggested by some researchers that specific heat capacity is associated with structure, this characterization is important [all main]. The images are also analyzed to study dispersion or agglomeration of NP in nanofluid and hence SEM is important to understand elements responsible for this anomalous behavior [28].

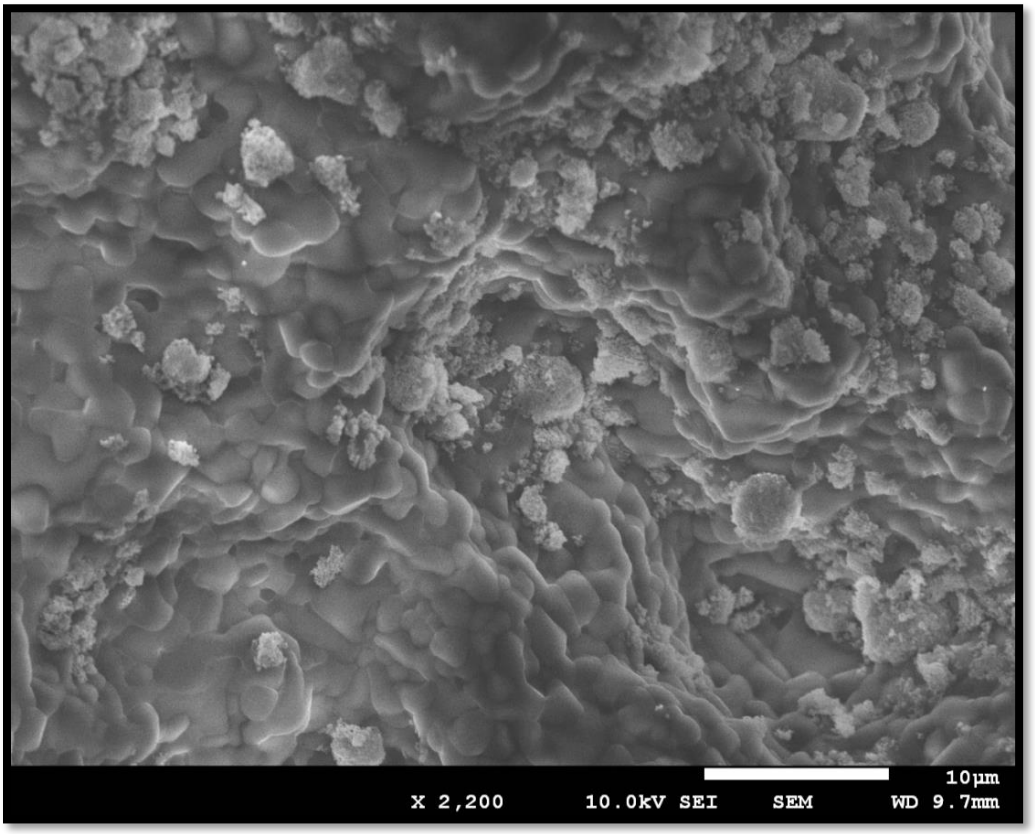

Figure 12: 1% Concentration of Al_2O_3 NP in MS.

MS is doped with 1% Al_2O_3 NP. SEM image is captured at 2,200 magnification and 10.0 kV power of electron gun. Figure 12 shows that NP are distributed over the region of image. The smooth surface which occupies most of the image and acts as a base is the molten salt. The small clusters distributed over the surface are Al_2O_3 particles. The sizes of NP observed in this image are not consistent. The NP used are of 80 nm in size. We can see many isolated nanoparticles. Clusters of size ranging from 1 μm to 5 μm are observed. But some clusters observed are as large as a few micrometers while some particles are present in nanometers. The dispersion of NP witnessed in this image seems to be uniform to some extent suggesting interaction between NP and molten salt at the interface between NP and MS, which may be responsible for increase in specific heat capacity. A highly magnified portion of figure 12 is shown in figure 13. The magnification power is 40,000. The Al_2O_3 particles are observed to aggregate together to form cluster with size in micrometers. The shape of Al_2O_3 particles is also observed to be similar to linkage as compared to spherical observed in some literature [21]. Microstructures are not observed in figure 13 as observed by Dudda, Shin and Shin and Banerjee. Well dispersed NP are observed and they are not agglomerated. We can observe many isolated NPs. Therefore a large surface of nanoparticles is available for interaction with MS. There is high surface energy available at this interface. There is interaction between NP and MS ions at the interface layer which enhances c_p of nanofluid as predicted by Cabedo, Ming Xi Ho and Lu Din Zihang. The nanolayer cannot be clearly seen around the surface of NPs but it is possible that it is present in liquid state and is responsible for enhancement of c_p value as predicted by Chieruzzi.

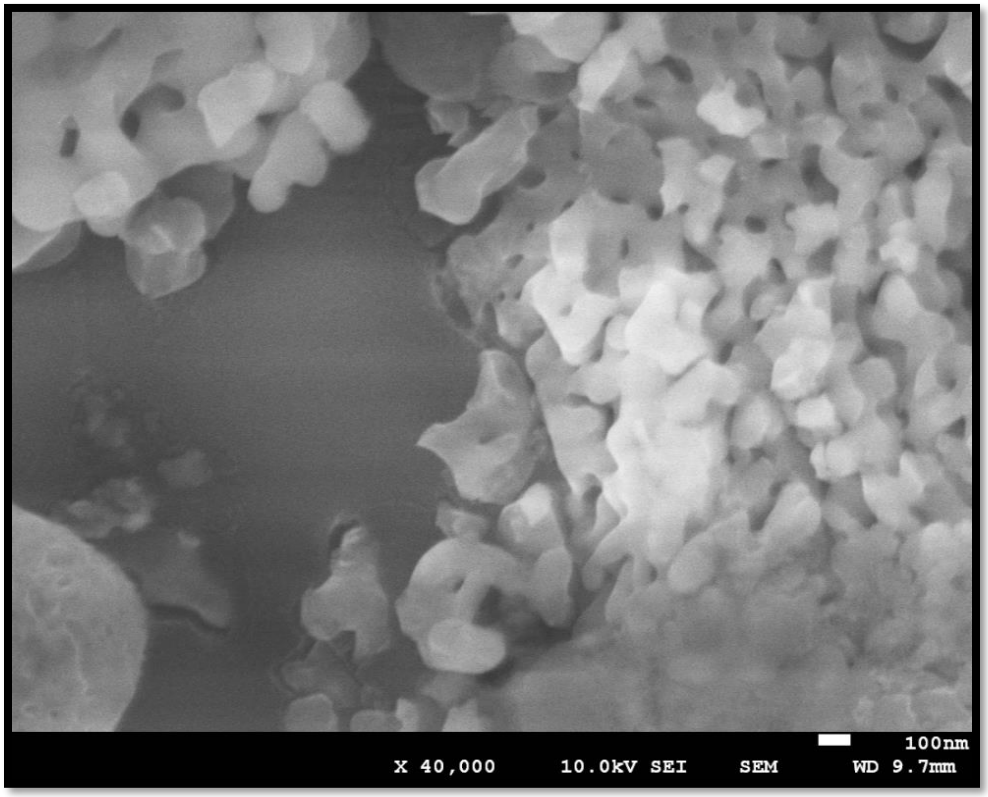

Figure 13: 40K Magnified Image of 1% Concentration of Al_2O_3 NP in MS.

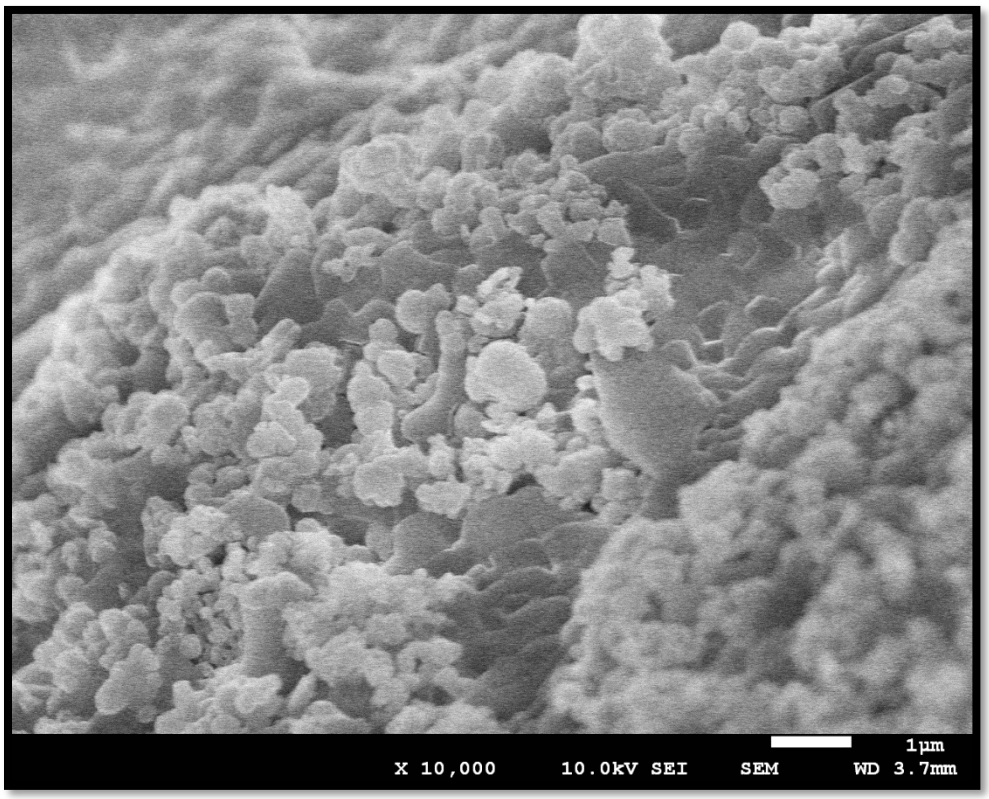

Figure 14: 0.5% Concentration for 25%-75% Sample.

Figure 14 shows majority of TiO_2 particles in molten salt. SEM image is captured at 10,000 magnification and 10.0 kV power of electron gun. Small amount of Al_2O_3 particles are also observed in this image. These particles are observed to be distributed uniformly over the entire region. The sizes of most of particles detected in figure 14 are in micrometers and few are in range of 200-500 nanometers in size. They are showing tendency to form clusters, but sizes of these clusters are in nanometers. So large surface area is available at the interface which is responsible for enhancement of c_p as explained earlier. The DSC calculation of this sample shows enhancement of c_p value by 8.7% in solid state and 8.9% in liquid state.

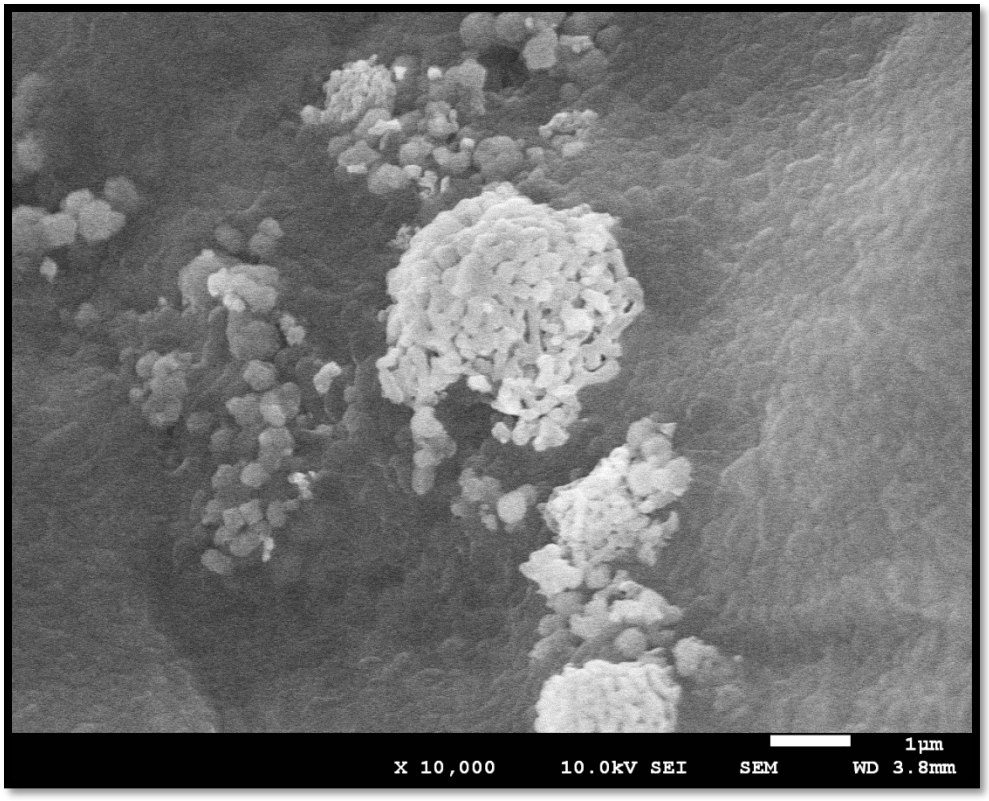

Figure 15: 1% Concentration for 50%-50% Sample.

Figure 15 shows SEM image of 50% Al_2O_3 and 50% TiO_2. This image is taken at 10,000 magnification. It is easier to differentiate between Al_2O_3 and TiO_2 particles as the Al_2O_3 particles appear to be brighter than TiO_2 particles. The reason being different surface energy which leads to a different contrast being transferred by electron beam [23]. Another way to differentiate them, is that Al_2O_3 particles are observed to be interlinked with chain like structure. Only few isolated particles of Al_2O_3 are seen. A cluster of Al_2O_3 particles is observed at center of image with another smaller one forming at bottom side of image. The TiO_2 particles are better distributed than Al_2O_3 and don't tend to form large clusters. It is important to observe that the Al_2O_3 and TiO_2 particles are not seen interacting for most part. The Al_2O_3 cluster is separate and TiO_2 particles are seen in another region. Some Al_2O_3 and TiO_2 are seen together and they can be seen in more detail in next zoomed in image.

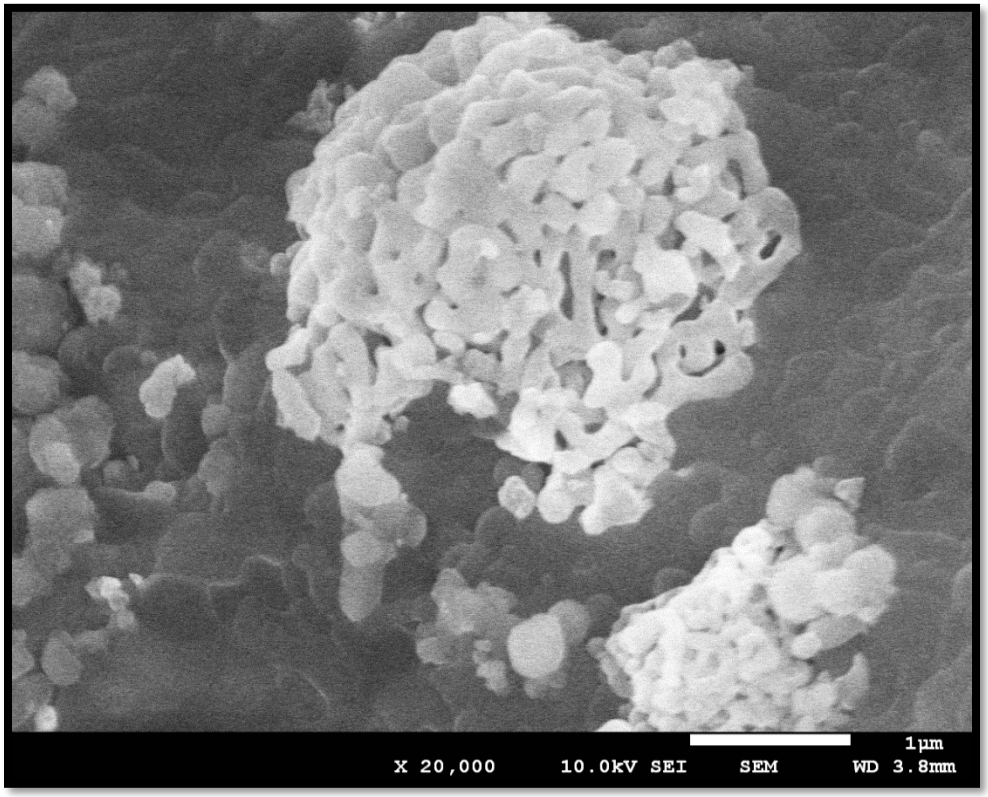

Figure 16: 20K Magnified Image of 1% Concentration for 50%-50% Sample.

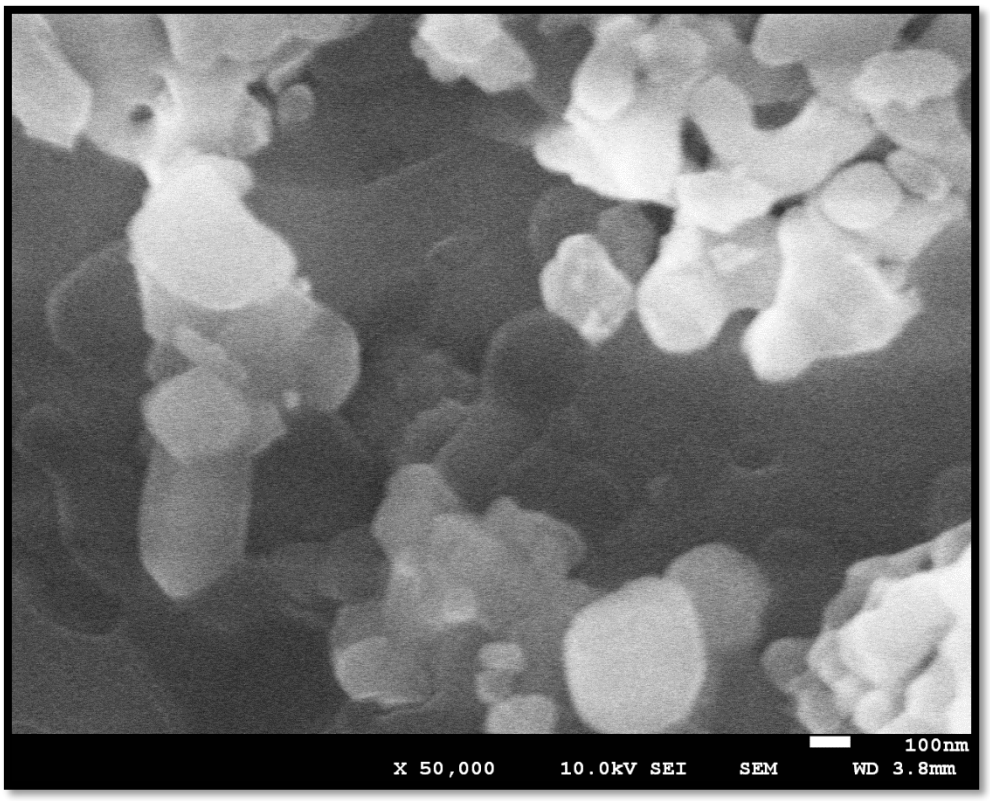

Figure 17: 50K Magnified Image of 1% Concentration for 50%-50% Sample.

The zoomed in image at 20,000 and 50,000 magnification power are shown in above figure. There is a small interaction observed on surface between Al_2O_3 and TiO_2 particles. The particles appear to be in contact and placed on surface of MS. The interaction of NP with each other will reduce the available surface area for MS to react with it. Also, the large cluster observed will be responsible for less particles available in nanometer size to give effect of nano size particles. The DSC results for this sample shows reduction in c_p value by 22.5% in solid state and 26.8% in liquid state and above mentioned interaction and aggregation observed could be accounted for this decrement in c_p value.

5.2 DSC Results for Specific Heat Capacity

Table 8: c_p of Nanofluids for Different NP and Concentrations

Type	Concentration	c_p solid	% Change	Uncertainty value	c_p liquid	% Change	Uncertainty value
MS (A)	0 %	1.356	0	±0.113	1.423	0	±0.110
MS + AL2O3 (B)	0.5 %	1.251	-7.7	±0.121	1.259	-11.5	±0.13
	1 %	Error	Error	Error	Error	Error	Error
	2.5 %	2.109	55.5	±0.798	2.926	105.6	±0.98
	5 %	1.384	2.0	±0.116	1.835	29.0	±0.127
MS + 75% Al_2O_3 +25% TiO_2 (C)	0.5 %	1.418	4.6	±0.184	1.374	-3.4	±0.246
	1 %	1.345	-0.8	±0.948	1.379	-3.1	±0.977
	2.5 %	1.216	-10.4	±0.735	1.212	-14.8	±0.735
	5 %	1.004	-26.0	±0.092	1.040	-26.9	±0.098
MS + 50% Al_2O_3 +50% TiO_2 (D)	0.5 %	1.345	-0.8	±0.295	1.180	-17.1	±0.3
	1 %	1.052	-22.5	±0.45	1.042	-26.8	±0.515
	2.5 %	1.274	-6.0	±0.471	1.536	7.9	±0.815
	5 %	1.424	5.0	±0.417	1.663	16.9	±0.608
MS + 25% Al_2O_3 +75% TiO_2 (E)	0.5 %	1.475	8.7	±1.17	1.550	8.9	±1.28
	1 %	1.241	-8.5	±0.45	1.286	-9.6	±0.546
	2.5 %	1.176	-13.3	±0.346	1.096	-23.0	±0.366
	5 %	0.808	-40.4	±0.39	0.834	-41.4	±0.407

The above table shows c_p values observed for solid state and liquid state. The different types of nanofluids are named alphabetically here onwards. The percent change is compared with sample A which is pure molten salt without NP. It can be observed that maximum increment is for sample B at 2.5% concentration for both solid and liquid phase and maximum decrement is for Sample E 5% over entire range of experimentation. No particular trend of increase or decrease in c_p is observed.

Consider results for c_p values in solid phase. Sample B shows c_p value reducing for 0.5% concentration but increasing thereafter for increasing concentration. Sample C shows an increase for 0.5% and decrease thereafter for c_p value compared with pure molten salt. Sample D shows a decreasing trend for 0.5% to 1% and then increasing trend from 2.5% to 5% concentration. Sample E shows trend similar to Sample C with an increase in c_p value for 0.5% and then reducing thereafter till 5% concentration. An important observation from this results is the re-occurrence of unimodal peaks. The peaks are at different concentrations and predict different values of c_p for each sample. Sample B shows that this peak might be present between 1% and 5% concentration. Sample C and E show the same between 0% and 1% and sample D shows that peak might be present above 5% concentration. Though the percentage change values are different for c_p in liquid phase, very similar trend can be observed for results of corresponding samples. Except for 0.5 % concentration of sample B in all other samples, for all concentrations, the effect of adding NP is more in liquid phase as compared to that in solid phase. The increment is more in liquid phase as compared to that in solid phase. The same is true in case of decrement also i.e. decrement is more in case of liquid phase as compared to that in solid phase.

The specific heat capacity of nanofluid is given by simple mixture rule / equation. As the c_p of nanomaterial is lower than c_p of molten salt we expect marginal decrease of nanofluid, as the concentration of NP is low 0.5 to 5%. But we obtained maximum enhancement 105.6% in case of sample B (2.5% concentration) for liquid phase, and maximum decrement obtained is 63% in case of sample E (5% concentration) for liquid phase. Similarly in case of solid phase maximum increment is 55.5% for sample B (2.5% concentration) and maximum decrement is 62.5% for sample E (5% concentration). Such large increment and decrement cannot be explained by simple mixture rule.

Different mechanisms were proposed in the literature reviewed for explaining this anomalous behavior of molten salt based nanofluids. One explanation is that c_p value of NP is higher than that of bulk material. The surface area of nanoparticle increases as its size is reduced. As the surface area increases the specific surface energies increase and subsequently the nanoparticles may have better thermal properties than the bulk material and this may contribute to the enhanced specific heat capacity of nanofluids [29]. Chieruzzi has suggested formation of nanolayer at solid / liquid interface. This layer has higher thermal properties than bulk liquid and it contributes to the enhancement of c_p value [12]. The nanoparticle dispersion plays major role on enhancement of c_p. The optimum dispersion of nanoparticles results in maximum surface availability. This dispersion can be different in solid and melted state providing different values of c_p for solid and liquid phase. The surface area can be calculated if SEM image shows the isolated nanoparticles and clusters of nanoparticles clearly. The low values of surface area availability corresponds to either low solid content with few particles or high solid content with agglomeration of particles. Hence the enhancement of c_p depends upon proper dispersion (availability of maximum surface area) and there exists an optimum concentration for which surface area is maximum for each type of nanoparticle [13].

If the concentration is lower than optimum we get low enhancement as less particles are available and if concentration is more than optimum, clusters of nanoparticles are formed which reduces the surface area. If the clusters are small it still enhances the c_p value. But as the concentration is increased the agglomeration becomes more intense and large size clusters are formed which may result in decrementing c_p value [14]. Similar findings were provided by Ho and Pan. The cluster size may also become large if we do not use proper process for preparing the nanofluid.

Another theory put forth by Shin and Banerjee suggests formation of a woven structure of molten salt eutectic which can be one of the factor for enhancement of specific heat. This nucleated phase is called as compressed phase and the specific heat of this compressed phase is much higher than that of base fluid. The mass of compressed layer formed is proportional to surface area available [20]. These structures are also called as fractal-like fluid nanostructures or needle like structures. But the mass fracture of these structures and their c_p value cannot be determined experimentally or theoretically [29]. In SEM images of present work, neither needle-like structure nor semi-solid layer formation is observed. But it is evident from results that concentration and type of NP are affecting c_p values.

The theory behind decrement in c_p value was suggested by Lu. He suggested formation of a solid-like nanolayer on the surface of nanoparticles. This layer is at the thermodynamic state between solid salt and liquid molten salt. The amount of mass and value of c_p of this nanolayer depends on the size of nanoparticle and its concentration. The low value of c_p of this nanolayer contributes to the decrement in specific heat capacity [17]. The other explanation is that if the clusters of large size are formed due to agglomeration of nanoparticles it decrements the specific heat value of nanofluid as the c_p value of nano bulk material is low [14]. The aggregation of NP in size of microns observed in SEM images which reduces the effect of dispersion of NP in MS and exhibit bulk c_p value. Effect of Brownian motion of NP does not play a significant role, since specific heat capacity is not a transport property [17].

In SEM images of present work, neither needle-like structure nor semi-solid layer formation is observed. But it is evident from results that concentration and type of NP are affecting c_p values. These factors suggests that pattern, dispersion and concentration of NP influence c_p values. SEM images suggests that sizes of NP interacting with surface of MS are varying and are

present in sizes of up to few microns also. Thus, it suggests that for each type of NP, a particular concentration will be able to give uniform dispersion and optimum pattern of NP which will provide maximum specific heat. Similar findings were provided by Ho and Pan.

5.3 DSC Results for Latent of Heat Fusion.

Table 9: Latent Heat of Fusion of Nanofluids for Different NP and Concentrations

Type	Concentration	Latent heat Solid	% Change	Latent heat liquid	% Change
MS	0%	111.88	0	-113.272	0
MS + Al_2O_3	0.5 %	111.688	-0.2	-115.371	1.9
	1 %	Error	Error	Error	Error
	2.5 %	106.446	-4.9	-113.74	0.4
	5 %	97.129	-13.2	-104.605	-7.7
MS + 75% Al_2O_3 +25% TiO_2	0.5 %	116.823	4.4	-124.202	9.6
	1 %	117.019	4.6	-122.652	8.3
	2.5 %	106.931	-4.4	-114.089	0.7
	5 %	101.635	-9.2	-105.125	-7.2
MS + 50% Al_2O_3 +50% TiO_2	0.5 %	108.979	-2.6	-119.32	5.3
	1 %	103.559	-7.4	-114.894	1.4
	2.5 %	108.65	-2.9	-117.401	3.6
	5 %	100.912	-9.8	-106.248	-6.2
MS + 25% Al_2O_3 +75% TiO_2	0.5 %	124.141	11.0	-130.641	15.3
	1 %	116.023	3.7	-123.654	9.2
	2.5 %	107.828	-3.6	-115.111	1.6
	5 %	106.958	-4.4	-112.863	-0.4

Latent heat of fusions show variation on adding NP to MS. The two heats of fusion found by experiments are for solid and liquid state. The maximum increment seen for solid state is 11% over pure MS at 0.5% concentration of sample E. Increment of 15% is observed for liquid state at same concentration for sample E. Maximum decreament in latent heats is observed at 5% of sample B which is 13.2% for solid and 7.7% for liquid. A general trend of decreasing latent heats is observed as concentration increases, but for most samples it is maximum at 0.5% concentration. Cheiruzzi has found maximum increment at 1% of Al_2O_3-SiO_2 hybrid nanofluid. The increase in atent heat supports application of thermal energy storage as heat storage is more per unit volume.

5.4 DSC Results of Melting Point and Freezing Point

Table 10: Melting and Freezing Points of Nanofluids for Different NP and Concentrations

Type	Concentration	MP	Change in MP	% Change	FP	Change in FP	% Change
MS	0%	223.313	-	-	231.394	-	-
MS + Al_2O_3	0.50%	222.747	0.6	-0.3	231.476	-0.1	0
	1%	Error			Error		
	2.50%	220.332	3	-1.3	230.677	0.7	-0.3
	5%	221.062	2.3	-1	230.422	1	-0.4
MS + 75% Al_2O_3 +25% TiO_2	0.50%	221.142	2.2	-1	232.087	-0.7	0.3
	1%	220.62	2.7	-1.2	231.396	0	0
	2.50%	220.327	3	-1.3	231.69	-0.3	0.1
	5%	220.084	3.2	-1.4	231.937	-0.5	0.2
MS + 50% Al_2O_3 +50% TiO_2	0.50%	222.035	1.3	-0.6	232.915	-1.5	0.7
	1%	221.843	1.5	-0.7	232.928	-1.5	0.7
	2.50%	222.437	0.9	-0.4	233.742	-2.3	1
	5%	219.933	3.4	-1.5	231.692	-0.3	0.1
MS + 25% Al_2O_3 +75% TiO_2	0.50%	220.748	2.6	-1.1	231.437	0	0
	1%	221.932	1.4	-0.6	233.147	-1.8	0.8
	2.50%	221.508	1.8	-0.8	233.584	-2.2	0.9
	5%	220.366	2.9	-1.3	231.76	-0.4	0.2

The melting point (also reffered to as onset temperature) shows consistent reduction as compared to pure MS. The minimum reduction in MP is 0.6°C at 0.5% concentration of sample B and maximum reduction is 3.4°C for sample D. Maximum reduction for sample B,C and E is 2.2°C, 3.2°C and 2.9°C respectively. The change in concentration of NP doesn't have a prominent effect on reduction in MP but reduction is maximum for higher concentration. The change in MP is different for different types of NP. We can observe that for concentrations

which give maximum enhancement in c_p, we get maximum reduction in melting point. Reduction in MP shows that phase change occurs at a lower temperature and hence is favourable for use in CSP. Similar trend was observed by cheiruzzi and showed maxumim reduction by adding 1% combination of Al_2O_3 and SiO_2. The freezing point however shows increment for most samples. This depicts that molten salt nanofluid will freeze at higher temperature and is not desirable for our application. Though this increment is not huge, a maximum increment is observed at 2.5% concentration of Sample D, whereas sample B and C show negligible change in freezing point. We can observe that for concentrations which give maximum enhancement in c_p, we obtain reduction in freezing point (or negligible increase), this is desirable change. General trend shows increment in FP with increasing concentration for all samples and similar to one observed by Chieruzzi.

Chapter 6

FUTURE SCOPE

Extensive experimentation is required to arrive at the optimum value of concentration to be used for each type of nanofluid. Since this concentration varies with type of nanoparticles, extensive experimentation needs to be done to find model for the same. Results of this work can be used by future researchers to establish an empirical relationship between enhancement in thermophysical properties and concentration of NP. Maximum enhancement in specific heat is obtained for Alumina nanoparticles at 2.5 % concentration. More experimental results should be conducted between 1% and 5 %to find the optimum concentration value. TiO_2 nanoparticles decrements the specific heat of molten salt hence experiments may be conducted by mixing some other nanoparticles with Al_2O_3.

Effect of thermal cycling may be studied in details. As the MS are used as HTF and TES, they will be under alternate heating and cooling cycles. Thermal cycling will cause decomposition of MS over a period of time and effect of adding NP on this can be studied in details. Also, changes in composition of MS for exposure to high temperature can be studied for finding change in decomposition temperature by adding NP.

Corrosion has been a key factor which affects the operation of CSP. Salts are observed to enhance effect of corrosion in pipes and instruments and lot of resources and extra coatings are added to avoid corrosion. Effect of adding NP on corrosion caused by MS can be studied in details.

Currently it has been established that chloride salts have higher decomposition temperature as compared to nitrate salts. The nitrate salts can go upto 550°C before starting to decompose. Whereas the chloride salt are found to be stable upto 800°C. These, if used can increase the Carnot cycle efficiency by a huge factor because of higher working temperature. Effect of adding NP in chloride salts can be studied to check if there is enhancement in thermophysical properties or rise in decomposition temperature.

REFERENCES

[1] Birol, F., World Energy Outlook, 2016, from https.//www.iea.org/newroom/news/2016/November/world – energy – outlook – 2016 html

[2] National Renewable Energy Lab, 2017, from https://www.nrel.gov/csp/solarpaces/

[3] Kuravi, S., Trahan, J., Goswami, Y., Rahman, M, M., Stefanakos, E, K., 2013, ‘‘Thermal Energy Storage Technologies and Systems for Concentrating Solar Power Plants’’, *Progress in Energy and Combustion Science*, **39,** pp. 285-319, http://dx.doi.org/10.1016/j.pecs.2013.02.001.

[4] Magal, B, S., 1990, *Solar Power Engineering*, 1st ed., Tata McGraw Hill Publishing Co. Ltd., Delhi, Chap. 6.

[5] Kearney D., Herrmann, U., Nava, P., Kelly, B., Mahoney, R., Pacheco, J., Cable, R., Blake, D., Price, H., and Potrovitza, N., 2003, ‘‘Overview on Use of a Molten Salt HTF in a Trough Solar Field’’, *NREL Parabolic Trough Thermal Energy Storage Workshop*, Golden, CO.

[6] Dudda, B., and Shin, D., 2013, ‘‘Effect of Nanoparticle Dispersion on Specific Heat Capacity of a Binary Nitrate Salt Eutectic for Concentrated Solar Power Applications’’, *International Journal of Thermal Sciences*, **69,** pp. 37-42.

[7] Cengel, Y, A., and Boles, M, A., 2015, *Thermodynamics, An Engineering Approach* 8th ed., McGraw – Hill Education, New York, Chap. 4.

[8] Nag, P, K., 2005, *Engineering Thermodynamics*, 4th ed., Tata McGraw – Hill Education, Delhi, Chap. 3.

[9] Verma, H, C., 1993, *Concepts of Physics*, Volume 2, 2016 ed., Bharati Bhavan Publisher and Distributors, New Delhi, India, Chap. 25.

[10] Tandon, O, P., and Singh, A, S., 2014, *Physical Chemistry*, 15th ed., G.R.Bathla Publications Pvt. Ltd. Delhi, India, Chap. 4.

[11] Rodgers, D, J., and Janz, G, J., 1982, ‘‘Melting – Crystallization and Premelting properties of $NaNO_3$-KNO_3. Enthalpies and Heat Capacities’’, *J. Chem. Eng. Data*, ***27***, pp. 424-428.

[12] Chieruzzi, M., Cerritelli, G, F., Miliozzi, A., and Kenny, J, M., 2013, ‘‘Effect of Nanoparticles on Heat Capacity of Nanofluids based on Molten Salts as PCM for Thermal Energy Storage’’, *Nanoscale Research Letters*, **8** (448), http://www.nanoscalereslett.com/content/8/1/448.

[13] Andreu-Cabedo, P., Mondragon, R., Hernandez, L., Martinez-Cuenca, R., Cabedo, L., and Julia, E, J., 2014, ‘’ Increment of Specific Heat Capacity of Solar Salt with SiO_2 Nanoparticles‘’, *Nanoscale Research Letters*, **9** (582), http://www.nanoscalereslett.com/content/9/1/582.

[14] Ho M, X., and Pan, C, 2014, "Optimal Concentration of Alumina Nanoparticles in Molten Hitec Salt to Maximize its Specific Heat Capacity", *International journal of heat and mass transfer*, **2014 70**, pp.174 -184

[15] Davies, A, G., and Thomson, J, M, T., 2007, *Advances in Nanoengineering Electronics, Materials and Assembly*, Volume 3, Royal Society series on Advances in Sciences, Imperial college Press, London, Chap. 1.

[16] O'Hanley, H., Buongiorno, J., McKrell, T., and Hu, L., 2012, ‘’Measurement and Model Validation of Nanofluid Specific Heat Capacity with Differential Scanning Calorimetry‘’, *Advances in Mechanical Engineering*, **2012** (181079), Hindawi Publishing Corporation, doi:10.1155/2012/181079.

[17] Lu, M, C., and Huang, C, H., 2013, ‘’ Specific Heat Capacity of Molten Salt-based Alumina Nanofluid‘’, *Nanoscale Research Letters*, **8** (292), http://www.nanoscalereslett.com/content/8/1/292.

[18] Zavoico A, B., 2001, "Solar Power Tower Design Basis Document", Revision 0, *Sandia National Laboratories,* USA.

[19] Zhang, L., Chen, X., Wu, Y., Lu, Y., and Ma, C., 2016, "Effect of Nanoparticle Dispersion on Enhancing the Specific Heat Capacity of Quaternary Nitrate for Solar Thermal Energy Storage Application", Solar energy materials and solar Cells, 157, pp. 808 – 813

[20] Shin, D., and Banerjee, D., 2013, "Enhanced Specific Heat Capacity of Nanoparticles Synthesized by Dispersing Silica Nanoparticles in Eutectic Mixtures". *Journal of Heat Transfer*, **135 (**032801) pp.1-8.

[21] Piriyawong, V., Thongpool, V., Asanithi, P., and Limsuwan, P., 2012, "Preparation and Characterization of Alumina Nanoparticles in Deionized Water Using Laser Ablation Technique", *Journal of Nanomaterials*, **2012** (819403), Hindawi Publishing Corporation, doi:10.1155/2012/819403.

[22] US Research Nanomaterials Inc, n.d., from http://www.us-nano.com/nanopowders.

[23] Zhou, W., and Wang, Z, L., 2007, *Scanning Microscopy for Nanotechnology*, 1st ed., Springer-Verlag New York, doi: 10.1007/978-0-387-39620-0, Chap. 1.

[24] Lee, R, E., 1993, *Scanning Electron Microscopy and X-ray Microanalysis*, 1st ed., PTR Prentice Hall, NJ 07632, Chap. 1.

[25] Mackenzie, S, J., Mulkern, T, J., and Beck Tan, N, C., 2001, *Material Properties of Bi-Modal Epoxy Networks*, 1st ed., Army Research Laboratory, Aberdeen Proving Ground, MD 21005, Chap. 2.

[26] Figliola, R, S., and Beasley, D, E., 2011, *Theory and Design for Mechanical Measurements,* 5th ed., John Wiley & Sons Inc., NJ 07030-5774, Chap. 5.

[27] Gomez, J, C., Glatzmaier, G, C., and Mehos, M., "Heat Capacity Uncertainty Calculation for the Eutectic Mixture of Biphenyl/ Diphenyl Ether Used as Heat Transfer Fluid", 2012, SolarPACES, Marrakech, Morocco.

[28] Chieruzzi, M., Crescenzi, T., Miliozzi, A., and Kenny, J, M., 2015, ''A New Phase Change Material Based on Potassium Nitrate with Silica and Alumina Nanoparticles for Thermal Energy Storage", *Nanoscale Research Letters,* **10** (273), https://www.researchgate.net/publication/279457261.

[29] Khanafer, K., Tavakkoli, F., Vafai, K., and AlAmiri, A., 2015, "A Critical Investigation of Anomalous Behavior of Molten Salt – based Nanofluids", *International communications in Heat and Mass Transfer,* **69,** pp.51 – 58.

APPENDIX

MATLAB Code for Conversion of % By Volume to % By Weight for a Mixture Containing Single NP and Combination of NP.

MATLAB code for nanofluid containing single NP.

```
clear all;
Cv = [0.005, 0.01, 0.025, 0.05];        %Volume concentration%
Db = 0.83;                              %Density of Base fluid g/cm3%
Dp = 3.97;                              %Density of Nano particle g/cm3%
Dn = (Dp*Cv)-(Db*Cv)+Db;                %Density of Nano fluid%
ADp = 3.97*ones (1,12);
Cm = (ADp./Dn).*Cv;                     %mass concentration%
PCm = Cm.*100;                          %mass concentration in '%' %
PCv = Cv.*100;                          %volume concentration in '%' %
```

Output Page:

	1	2	3	4
1	1.0445	2.0777	5.1107	9.9549

Figure 18: Output Page Showing % Volume to % Weight Conversion

The conversion of 0.5%, 1%, 2.5% and 5% by volume gives 1.0445%, 2.0777%, 5.11% and 9.9549% by weight respectively. These values were used for measuring mass of NP while mixing in molten salt for particular concentration.

MATLAB code for mixing of two NP and base fluid.

```
prompt1= 'Enter the volumetric concentration of Al2O3';
prompt2= 'Enter the volumetric concentration of TiO2';
prompt3= 'Enter the mass of mineral oil';
Cal = input(prompt1);      %Vol% of Al2O3%
Cti = input(prompt2);      %Vol% of TiO2%
mmo = input(prompt3);   %mass of Molten salt %
pmo  = 1.89;                %density of Molten salt %
pal = 3.97;                 %density of Al2O3%
pti = 2.4;                  %density of TiO2%
p= ((1-Cal)/pal);
q = -(Cal/pti);
r = (-Cti/pal);
s = ((1-Cti)/pti);
t = (mmo/pmo)*Cal;
u = Cti*(mmo/pmo);
xy= [p q; r s]\[t;u]
```

Sample Output values

```
>> Mixture_Code_hybrid_NF
Enter the volumetric conentration in % of Al2O3 = 0.005
Enter the volumetric conentration in % of TiO2 = 0.005
Enter the mass of molten salt in gm = 5

xy =

    0.0530
    0.0321

>>
```

Figure 19: Sample Output for Conversion from % By Volume to % By Weight for Hybrid Nanofluid

The mixture code for hybrid Nanofluid converts the % by volume to % by weight for the mixture. These % by weight values are used to measure the molten salt and NP and then use for preparation of hybrid nanofluid. Figure 19 shows a sample calculation for 1% concentration of 50% Al_2O_3 - 50% TiO_2. Since the total concentration is 1 % there is 0.5% of Al_2O_3 and 0.5% of TiO_2. These values are input for prompt command as shown in figure 19. We want to prepare a sample of 5gm by weight. Hence mass of molten salt is 5 gm is input shown in above figure. The output value is for Al_2O_3 and TiO_2 in gm respectively. These are the actual values required to measure and add to molten salt while preparation of hybrid nanofluid.